Analyst

Advanced manufacturing of nanoparticle formulations of drugs and biologics using microfluidics

Journal:	*Analyst*
Manuscript ID	AN-CRV-10-2023-001739.R1
Article Type:	Critical Review
Date Submitted by the Author:	27-Nov-2023
Complete List of Authors:	Shen, Yingnan; Purdue University, Mechanical Engineering Gwak, Hogyeong; Purdue University, Mechanical Engineering Han, Bumsoo; Purdue University, Mechanical Engineering

ADVANCED MANUFACTURING OF NANOPARTICLE FORMULATIONS OF DRUGS AND BIOLOGICS USING MICROFLUIDICS

Yingnan Shen[a,*], Hogyeong Gwak[a], and Bumsoo Han[a,b,*]

[a] School of Mechanical Engineering, Purdue University, West Lafayette, IN 47907, USA

[b] Purdue University Institute for Cancer Research, West Lafayette, IN, 47907, USA

*Co-Corresponding Authors

Yingnan Shen, Ph.D.

585 Purdue Mall, West Lafayette, IN 47906, U.S.A.

E-mail: shen453@purdue.edu

And

Bumsoo Han, Ph.D.

585 Purdue Mall, West Lafayette, IN 47906, U.S.A.

E-mail: bumsoo@purdue.edu

Tel: +1-765-494-5626

ABSTRACT

Numerous innovative nanoparticle formulations of drugs and biologics, named nano-formulations, have been developed in the last two decades. However, methods for their scaled-up production are still lagging, as the amount needed for large animal tests and clinical trials is typically orders of magnitude larger. This manufacturing challenge poses a critical barrier to successfully translating various nano-formulations. This review focuses on how microfluidics technology has become a powerful tool to overcome this challenge by synthesizing various nano-formulations with improved particle properties and product purity at large quantities. This microfluidic-based manufacturing is enabled by the microfluidic mixing capable of the precise and continuous control of the synthesis processes of nano-formulations. We further discuss the specific applications of hydrodynamic flow focusing, staggered herringbone micromixer, T-junction mixer, micro-droplet generator, and glass capillary on various types of nano-formulations of polymeric, lipid, inorganic, and nanocrystals. Various separation and purification microfluidic methods to enhance the product purity are reviewed, including acoustofluidics, hydrodynamics, and dielectrophoresis. We further discuss the challenges of using microfluidics by broader research and industrial communities. We also provide the future outlooks of its enormous potential as a decentralized approach for manufacturing nano-formulations.

1. Introduction

Numerous innovative nanoparticle formulations have been developed for targeted and improved drug deliveries [1-3]. Early efforts have been focused on chemotherapeutic drugs for oncology applications. However, many of these formulations were developed and tested using preclinical small animal models. It is still challenging to translate for large animal tests and clinical trials. For now, only twenty-eight nanoparticle therapeutics (including COVID-19 vaccines with emergency use authorization) have been approved for clinical use [4-7]. A major hindrance lies in the dramatical increase of the amount of nanoparticle (NP) needed for clinical trials compared to small animal tests. For example, antitumor nano-formulations may require hundreds of grams of NPs for a Phase 1A clinical trial [8, 9]. Thus, scaling up for production is one of the technical gaps to research and test many nano-formulations at more clinically relevant settings.

The large-scale production is technically challenging as batch-to-batch variations of physiochemical properties may occur due to the polydispersity of NPs which can induce inconsistency in preclinical or clinical trials [10, 11]. The conventional batch production methods or reactors include solvent evaporation for polymeric NPs [12-14], extrusion for lipid nanoparticles (LNPs) [15, 16], and static mixer for nanocrystals [17-19]. These batch synthesis methods operate at the millimeter or even centimeter scale, resulting in a uniform mixing environment where the local fluctuations of

concentration occur and leads to the formation of NPs with large size and wide size distribution. NP size and shape are crucial physicochemical properties to control during the synthesis process as it directly influences the therapeutic efficacy of NPs, such as in vivo biodistribution and retention ability in tissues, as well as the uptake and clearance by macrophages [20-22]. The batch production methods may generate polymeric NPs with uncontrolled size and limited drug loading resulting in short biodistribution [4, 23], LNPs with the high polydispersity index (PDI) leading to limited tissue penetration [24, 25]; worse, the nanocrystals are produced by batch methods in a wide range of size depending on the type of hydrophobic drugs [26-28]. Therefore, microfluidic platforms are developed and employed to scale up the manufacturing of nano-formulations. The utilization of microfluidics not only avoids labor-intensive multistep processes for research labs, but also avoids batch-to-batch variations with its continuous manner of NP synthesis. The microfluidics also provides precise control of synthesis process which allows convenient modification of physicochemical properties of NPs.

Firstly, we explain how microfluidics can bring high consistency and reproducibility to nano-formulation synthesis by controlled rapid mixing of pico- to nanoliter volumes of fluids in the perspective of separating the NP formation stages of nucleation, growth, and aggregation. Then we specifically introduce the microfluidic mixing techniques of hydrodynamic flow focusing, staggered herringbone micromixer, T-junction mixer, micro-droplet generator, and glass capillary, as well as their applications to the synthesis of polymeric NPs, lipid NPs, inorganic NPs, and nanocrystals with improved physical properties and in vivo behaviors. Microfluidic separation techniques to separate and purify the nano drugs and biologics are also summarized, including both the passive and active techniques of acoustofluidics, hydrodynamics, and dielectrophoresis. Finally, we discuss the current challenges of the utilization of microfluidics by broader research and industrial communities due to high entry level and fabrication complexity; its enormous potential as a decentralized approach for the manufacturing of NP-based drug formulations, ideally meeting the specific needs of individuals.

2. Mechanisms of formation of drug nanoparticles on microfluidics

The microfluidics techniques of hydrodynamic flow focusing, staggered herringbone micromixer, T-junction mixer, micro-droplet generator, and glass capillary have precise control over nanoliter volumes of fluid in the device with microscale dimensions, and thus achieve short microfluidic mixing timescale in the order of milliseconds which enables the control of the nanoprecipitation-based NP formation process [29]. Specifically, the concurrent occurrence of NP formation stages of nucleation, growth, and aggregation induces significant batch-to-batch variations to the conventional batch methods [30, 31]; By comparison, microfluidic platforms do a better job to separate the three NP stages with their short mixing timescales [32-36]. The mixing timescale related mechanism explaining different NP formation dynamics induced by microfluidic mixing and batch mixing is illustrated in

Figure 1. The microfluidic mixing timescale (τ_m) can be tuned to be shorter than the drug's nucleation timescale (τ_n), so the drug solute concentration quickly exceeds the saturation concentration (c_s) and reaches the critical nucleation concentration (c_n), leading to the generation of evenly distributed precursors for nucleation (prenucleation drug molecule clusters). Then the concentration of drug solute quickly drops when homogeneous nucleation is initiated. Homogeneous nucleation dominates over the particle growth in consuming the remaining drug molecules or clusters, which fulfills the synthesis of small and uniform NPs. The batch mixing timescale (τ_m') is longer than τ_n, which means the mixing is still not completed when the nucleation starts. Nuclei are generated but there are still a large amount of solutes dissolved in the organic phase, so the particle growth dominates over the heterogeneous nucleation in consuming the remaining drug molecules, resulting in NPs with higher size and PDI.

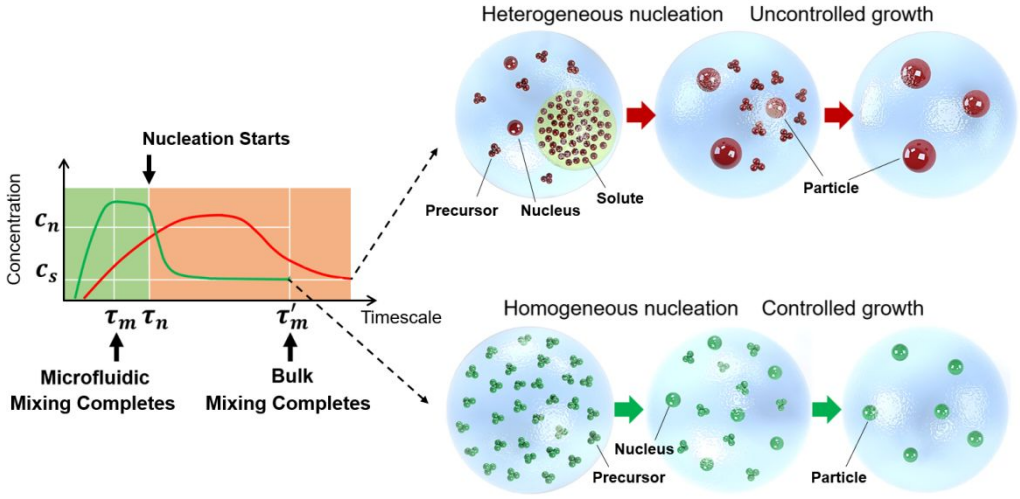

Figure 1. Schematical explanation of the different NP formation dynamics induced by microfluidic mixing and batch mixing. The shorter microfluidic mixing timescale (τ_m) than the drug's nucleation timescale (τ_n) (i.e., green line) induces homogeneous nucleation and controlled growth of particles, while the longer mixing timescale (τ_m') than τ_n such as batch mixing (i.e., red line) leads to heterogeneous nucleation and uncontrolled growth of particles.

The precisely fabricated microfluidic channels with dimensions of tens to hundreds of micrometers allow high levels of control of the fluids in the laminar flow regime. The microfluidic mixing mechanism is based on the interdiffusion of solvent molecules obtained by means of laminar flows. Hence, the microfluidic mixing can be characterized by the Reynolds number, *Re*, and the Peclet number, *Pe*.

$$Re = \frac{\rho u L}{\mu} \qquad (1)$$

where ρ and μ are the density and viscosity of the fluid, respectively, u is the flow speed, and L is the characteristic length of the channel. The Reynolds number is a dimensionless quantity characterizing flow patterns, which indicates the occurrence of turbulent flow when Re > 2000 – 4000 [37].

$$Pe = \frac{uL}{D} \quad (2)$$

where *D* is the diffusivity. The Peclet number describes the relative importance of the mass transport by diffusion (across the channel) and by convection (along the channel). In order to generate predictable mixing patterns, the microfluidic mixing is mostly designed to operate at Re < 2000 to avoid turbulent flows which have random streamlines [31, 38]. Our previous work on microfluidic synthesis of drug nanocrystals shows the streamline distribution in a microfluidic mixing device in the Reynolds number range of 5–250 where straight and parallel streamlines are present at Re = 5 while micro vortices can occur at Re = 25 in the water-ethanol mixing region [39]. The constraint of the Reynolds number leads to the upper limit of the Peclet number of 250 – 2500 [40]. The precise control of the mixing between fluids is not possible using conventional batch methods but can be achieved in microfluidics in a continuous manner with predictable mixing efficiency, which enables the control of the NP formation processes of nucleation, growth, and aggregation, and thus the limitations on uniformity and consistency of NP characteristics can be overcome on microfluidic synthetic platforms.

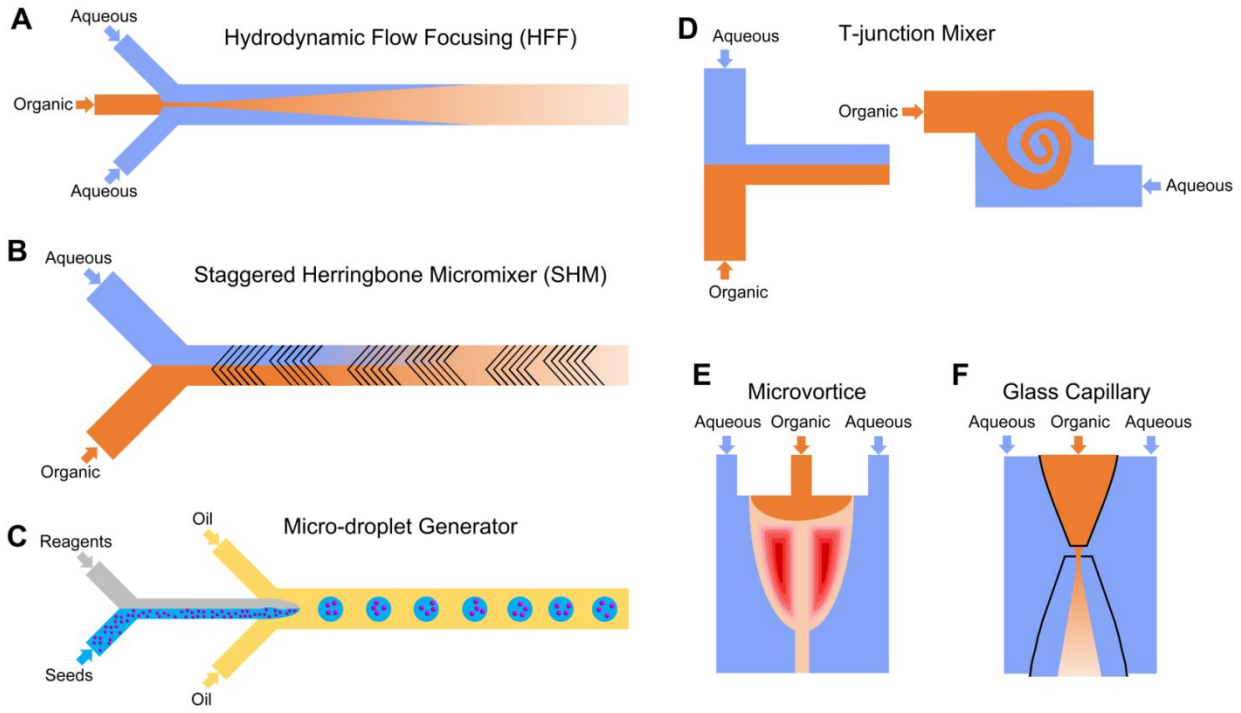

Figure 2. Schematic of the microfluidic mixing techniques for the synthesis of nanomedicine. (A) Hydrodynamic flow focusing (HFF). (B) Staggered herringbone micromixer (SHM). (C) Micro-droplet generator. (D) T-junction mixer. (E) 3D flow focusing with microvortices. (F) Glass capillary.

Microfluidic platforms have been utilized to produce NPs with a smaller size, narrower size distribution (i.e. smaller PDI), and improved drug loading and encapsulation efficiency [23]. To achieve this, nanoprecipitation is induced in the microchannel via rapid mixing of solvent and anti-solvent. Several microfluidic mixing techniques have been developed without the involvement of external fields, including hydrodynamic flow focusing (HFF), staggered herringbone micromixer (SHM), T-junction mixer, micro-droplet generator, and glass capillary. These microfluidic mixing methods are employed to produce various types of NPs including polymeric NPs, LNPs, inorganic NPs, and drug nanocrystals. The low Reynolds numbers (generally less than 100) [41] indicate steady state and fully developed laminar flow regimes during microfluidic mixing, and hence the mass transfer can be considered to depend solely on diffusion. The mixing time (τ_m), which is a measure of the solvent exchange efficiency, quadratically depends on the diffusion length between solvents. τ_m can be defined as

$$\tau_m = \frac{x^2}{2D} \quad (3)$$

where x is the diffusion length and D is the diffusion coefficient [42]. Therefore, the diffusion-based microfluidic mixing methods rely on the reduce of diffusion length for the control of the mixing time to provide homogeneous environment for NP formation.

The HFF is a powerful tool to reduce the diffusion length between the mixing solvents with a stable control. As schematically shown in **Figure 2A**, an HFF is commonly a three-inlet microfluidic device which generates a central flow with side flows. The flow regime of HFF develops when fluids with different velocities are introduced to the mixing channel side by side [43]. The central fluid flows at a much lower velocity than the side fluid in the same channel. As a result, the central fluid (organic phase) containing the samples of interest is sheathed into a thin sheet by the side fluid (aqueous phase) to achieve fast mixing between the two fluids. **Figure 2B** shows the schematic structure of SHM. The microfluidic SHM has two inlets and utilizes repeated patterns of asymmetric protrusions to induce passive mixing by chaotic stirring, which greatly reduces the diffusion length between the two fluids [44, 45]. Chaotic stirring can be induced by the asymmetric protrusions at low Reynolds numbers (*Re* < 100) [46]. Efficient mixing of the organic and aqueous fluids can be achieved within 10 or 15 cycles of the repeated patterns [47]. **Figure 2C** shows the microfluidic droplet-based mixing which confines the chemical reactions to picoliter-sized droplets. The droplet generators are commonly used for inorganic NP synthesis [48]. The aqueous droplets containing the seed of NPs and other reagents for reaction are generated in the form of water-in-oil emulsions. In a T-junction mixer, two fluids flow directly toward each other with a perpendicular output. The simple T-junction

mixing shown in **Figure 2D** (left) is not able to reduce the diffusion length when it operates with the stratified laminar flows [49]. To enhance the mixing, the T junction can be designed with dimensions in the millimeter range and operates at turbulent or transitional conditions (Re > 2000) [50]. To enable the T junction to work in the microfluidic mixing scenario (Re < 100), the vortex micro T-mixer has been developed to form vortex flows at low Reynolds numbers [51, 52]. Figure 2D (right) shows the generation of vortex flows in the mixing channel by two fluids flowing through non-aligned inlets. The two-dimensional HFF (Figure 2A) squeezes the central fluid horizontally but not vertically. **Figure 2E** shows the microfluidic device enabling the three-dimensional (3D) squeeze of the central fluid with the generation of microvortices upstream of 3D flow focusing [53, 54]. The benefit of the 3D flow focusing lies in the elimination of the interface between the central fluid and the wall of the microchannel, which can significantly reduce the NP attachment and minimize the risk of channel clogging [55-57]. Another approach for 3D flow focusing is the microfluidic device of glass capillary (**Figure 2F**). The glass capillary device is fabricated by inserting the tapered cylindrical capillaries into a square capillary [58]. Similar to the HFF on 2D, the organic solvent is the inner phase, and the aqueous solution is the outer phase. The inserted glass capillary positions the organic solvent at the center of the mixing channel in all directions. Thus, the organic-aqueous interface, where the NPs are predominantly formed, is fully displaced from the walls of the mixing channel [59].

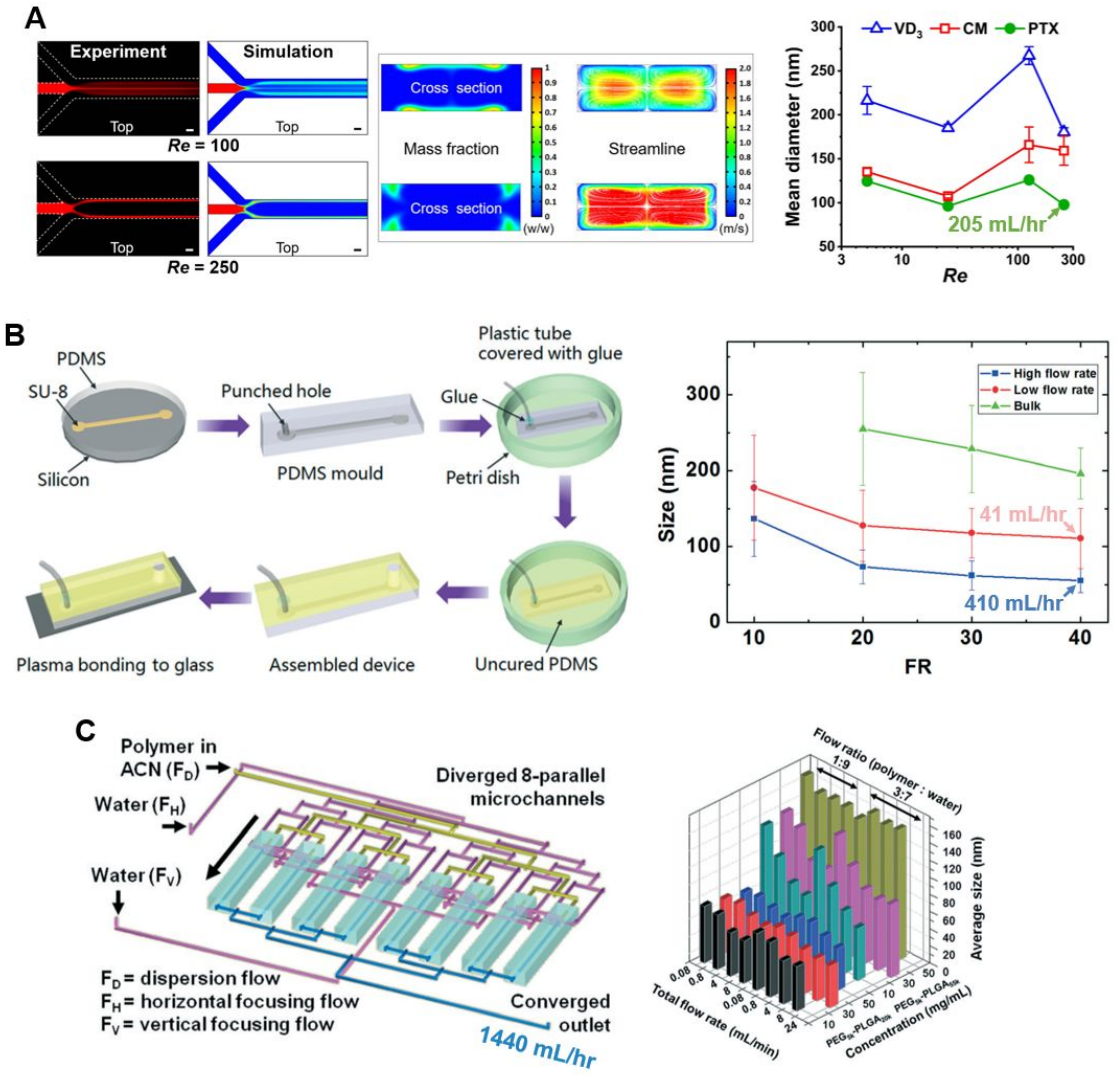

Figure 3. Scale-up strategies for the microfluidic synthesis of NPs. (A) Timescale-based optimization of the flow rate conditions in a single microchannel. A flow rate of 205 mL hr^{-1} was achieved to produce quality-controlled NPs of hydrophobic drugs with a size of approximately 100 nm. Reprinted with permission from ref. [39]. Copyright 2023 Elsevier. (B) Enhanced convective mixing in a microchannel with pressure-tolerant designs. A flow rate of 410 mL hr^{-1} was achieved to produce PLGA NPs while maintaining their small size of 55 nm. Reprinted with permission from ref. [60]. Copyright 2013 Royal Society of Chemistry. (C) Pressure-tolerant microfluidic device which parallels multiple microchannels. The total flow rate of eight microchannels reached 1440 mL hr^{-1} which enabled a mass production rate up to 1300 mg hr^{-1}. Reprinted with permission from ref. [61]. Copyright 2014 Royal Society of Chemistry.

To scale up the production of NPs at clinically or industrially relevant levels, three strategies can be adopted in microfluidic settings. First, the flow rate through the microchannel can be regulated

according to the timescale-based mechanism discussed in Figure 1. This strategy enables the determination of the optimal flow rate range to achieve high throughput synthesis of NPs while maintaining the quality of NPs including size and drug loading. As shown in **Figure 3A**, our group proposed a timescale-based mechanism to optimize the HFF conditions for both synthesis quality and throughput. We noticed an increase in NP size and a decrease in drug loading when the flow rate was increased to 102.5 mL hr^{-1} due to the accumulation of organic solvent in the bifurcated streams. This issue could be resolved when the flow rate was further increased to 205 mL hr^{-1}, while maintaining a good quality of NPs with approximately 100 nm in size, 0.1 in PDI, 70% encapsulation efficiency, as well as 50% drug loading [39]. The second strategy to further increase the throughput is to introduce strong convective mixing to the microchannel. However, a high inlet flow pressure is required, and high-pressure capacity of the tubing interconnection needs to be developed to avoid the liquid leakage. As shown in **Figure 3B**, a robust tubing method was developed to sustain a pressure of up to 4.5 MPa. This high-pressure tubing technique allows for strong convective mixing at the high flow rate of 410 mL hr^{-1}, resulting in size-controlled synthesis of small PLGA NPs of 55 nm in diameter with a good dispersion. The mass production of PLGA NPs can reach 200 – 800 mg hr^{-1} [60]. Combining with the first two strategies, the third strategy to scale up the throughput is to parallel the microchannels. In **Figure 3C**, a pressure-tolerant (up to 16 MPa) 3D-HFF device paralleling eight microchannels was fabricated to prepare PLGA NPs. The NP size was reproducibly controlled between 50 and 150 nm at the flow rate up to 1440 mL hr^{-1} which enabled a mass production rate of approximately 1300 mg hr^{-1} [61]. These scale-up strategies show potential to meet the clinical or even industrial purposes via microfluidic synthesis.

3. Microfluidic synthesis and separation strategies for nano-formulations

The nano-formulations can encompass both organic and inorganic materials of synthetic or natural origin for nanomedicine, and hence can be classified as organic or inorganic NPs [62]. Inorganic NPs offer great opportunities in nanomedicine serving as therapeutic or imaging agents. The commonly used materials for inorganic NP include metals, metallic oxides, and semiconductors [63]. Organic NPs can be further divided into polymeric NPs, lipid NPs, and (small molecule) drug nanocrystals. Here we discuss the microfluidic synthetic strategies for these different types of nano-formulations, as well as the microfluidic separation and purification of nano drug and biologics.

3.1. Polymeric NPs

Polymeric NPs is one of the most studied formulations as a nanomedicine from the applications of drug delivery to imaging. Poly (lactic-co-glycolic acid) (PLGA) stands out as the most clinically advanced polymer for its hydrophobicity, which enables easy nanoprecipitation for NP formation and loading of hydrophobic drugs (such as paclitaxel) into PLGA NPs [64]. PLGA also shows good

biodegradability and biocompatibility with negligible effects to organisms in most cases [65, 66]. Another good example is polyethylene glycol (PEG), which has become the most popular polymeric molecule for the coating of NPs [67]. PEG makes the NPs sterically stabilized by forming a hydrophilic layer on the surface of NPs [68]. The controlled release properties of polymeric NPs rely on the controlled properties of polymers which alter the release profiles of the encapsulated drugs [69]. The conventional batch method of solvent evaporation involves multiple time-consuming steps of the production and post processing of emulsions; and moreover, the batch produced polymeric NPs typically have big sizes of over 150 nm, limited drug loading, as well as significant batch-to-batch variations.

The microfluidic synthesis of polymeric NPs can be conducted in different devices of HFF, SHM, micro-droplet generator, and glass capillary. HFF is the most commonly used microfluidic method in polymeric NP studies, where a central stream of polymer-containing organic solvent is squeezed by the side aqueous streams flowing at a much higher speed. **Figure 4A** shows a study to synthesize PLGA-PEG NPs by rapidly mixing polymer-acetonitrile solutions and water using the HFF device [23]. The PLGA-PEG NPs prepared by batch mixing method increased dramatically in size with the addition of free PLGA to the precursor solution, but the size of NPs produced by the HFF method remained relatively unchanged with the increase of PLGA concentration up to 50 mg mL^{-1}. Moreover, the half life of the encapsulated drug of docetaxel is longer in the microfluidic NPs than that in the batch NPs (19 hr *versus* 11 hr). **Figure 4B** shows a study which proposed a variation of the design of HFF [70]. The HFF chips were manually folded to form the geometries of arc and double spiral to facilitate the mixing. The combination of HFF and 3D curved microchannels was found to significantly reduce the mixing time which enabled the synthesis of doxorubicin (DOX)-loaded PLGA with good size control at a higher throughput. The HFF-synthesized PLGA NPs were also found to significantly improve the stability of the encapsulated drug of curcumin with a half-life of 2 days; in comparison, the half-life the free drug of curcumin was as short as 30 minutes [71]. To avoid the channel clogging by polymer aggregates, PDMS-based 3D HFF devices were developed to reduce the organic stream-channel wall interface and showed no channel fouling after running the synthesis of PLGA-PEG NPs for over 10 minutes [55].

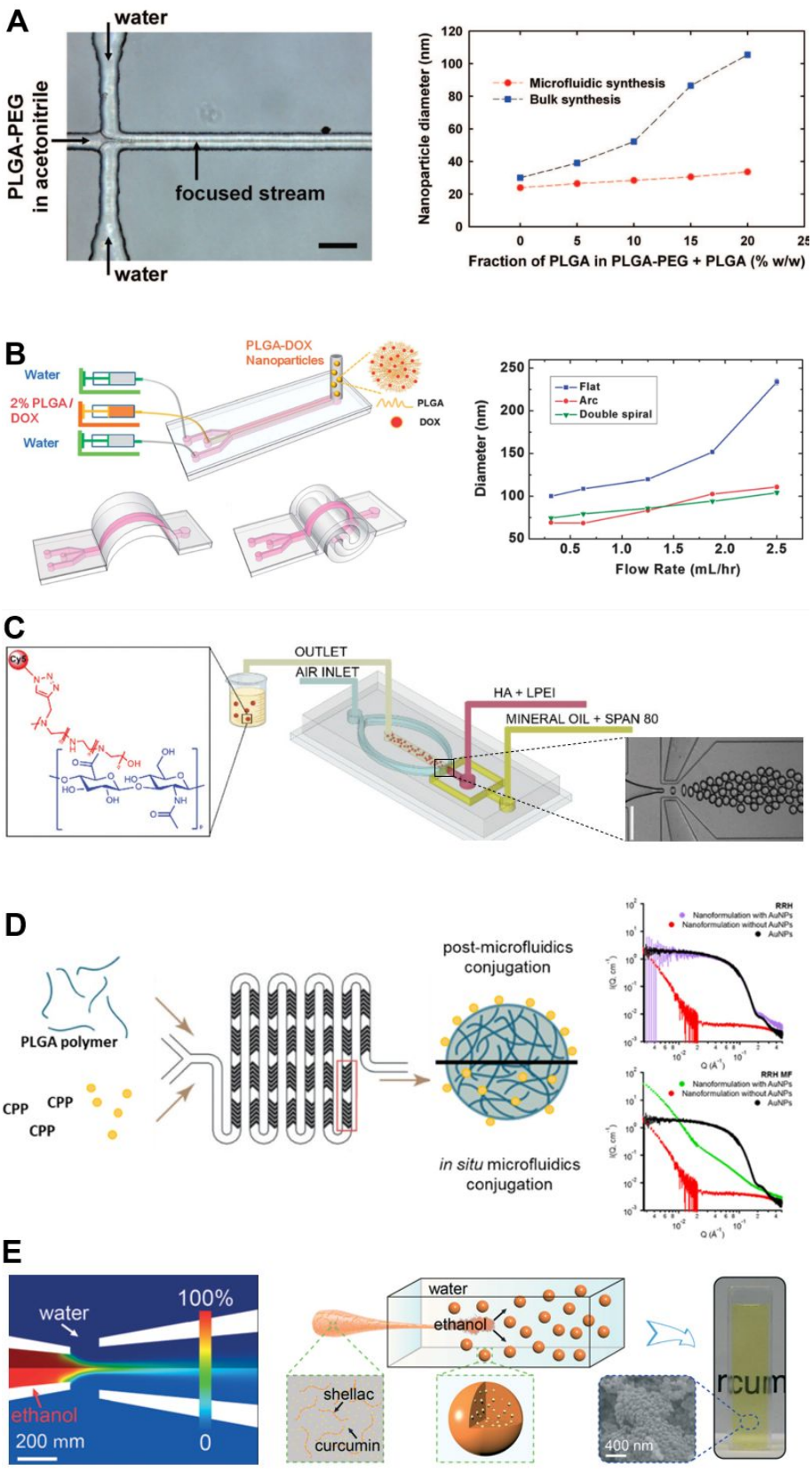

Figure 4. Microfluidic methods for the synthesis of polymeric NPs. (A) Hydrodynamic flow focusing (HFF). Improved polymeric NP properties by HFF synthesis with much less increase of particle size with the increase of PLGA concentration compared to batch NPs (< 50% versus > 200%), leading to

a longer half-life of the encapsulated drug of docetaxel. Reprinted with permission from ref. [23]. Copyright 2008 American Chemical Society. (B) Spiral HFF. Combination of HFF and 3D curved microchannels achieves good size control of PLGA NPs at ten times higher throughput compared to the flat chip. The half-life is tens of times longer than the free drug of curcumin. Reprinted with permission from ref. [70]. Copyright 2014 Royal Society of Chemistry. (C) Micro-droplet generator. Highly monodispersed polymeric NPs are formed within the micro-droplets with a very small PDI of 0.015. Reprinted with permission from ref. [72]. Copyright 2022 Royal Society of Chemistry. (D) Staggered herringbone micromixer (SHM). PLGA NPs prepared with SHM shows improved in-particle distribution of the encapsulated CPPs. Reprinted with permission from ref. [73]. Copyright 2019 Elsevier. (E) Glass capillary. The short mixing time of 9 ms in the glass capillary device enables a high encapsulation efficiency of 98% for curcumin. Reprinted with permission from ref. [58]. Copyright 2019 Royal Society of Chemistry.

The study shown in **Figure 4C** provided a synthesis of polymeric NPs via droplet-based microfluidics [72]. The polymers of hyaluronic acid (HA) and linear polyethyleneimine (LEPI) were covalently crosslinked in each droplet to produce highly monodispersed polymeric NPs with tunable sizes of 92 – 190 nm and a very small PDI of 0.015. The release of the encapsulated DOX exhibited an enhanced antiblastic effect even at sublethal dosages, highlighting the applicability of this droplet-based microfluidic method in nanomedicine scenarios. The efficient production of PLGA NPs is also feasible using the mixer of SHM. The study in **Figure 4D** optimized the total flow rate (TFR) and flow rate ratio (FRR) of the aqueous and organic solutions introduced to the SHM device for the synthesis of PLGA NPs tagged with cell-penetrating peptides (CPP). The distribution of the CPPs (Au-labeled) throughout the PLGA NPs was only observed when the PLGA NPs were prepared with the conjugation approach of in situ SHM [73]. The example of the application of the glass capillary, as a variation of 3D HFF, on the synthesis of polymeric NPs is provided in **Figure 4E** [58]. The curcumin-loaded shellac NPs were produced by injecting the ethanolic polymer solution from the tapered cylindrical capillary into the water-containing outer square capillary. The mixing time was estimated at 9 ms with a mixing length of 1.6 mm when the glass capillary device was operating at the parameters of TFR = 20 mL hr^{-1} and FRR = 40. A high encapsulation efficiency of 98% for curcumin was achieved indicating that the glass capillary synthetic method can be robust and reproducible encapsulate hydrophobic drugs in biocompatible polymeric NPs. Not only encapsulation efficiency, but also release kinetics and anticancer effect of the polymeric NPs can be improved when prepared using the microfluidic methods. For example, one study encapsulated gemcitabine in PLGA NPs using the microfluidic mixing device of HFF [74]. Compared to the gemcitabine-loaded PLGA NPs prepared by the double-emulsion/solvent evaporation method, the encapsulation efficiency was

increased by two-fold; moreover, the release of gemcitabine was slower, and more potent cytotoxicity was observed against the human breast cancer cells of MCF-7.

3.2. Lipid NPs

Lipid NPs (LNPs) or liposomes can be used to deliver hydrophobic drugs by encapsulating them in the lipid bilayer [75]. LNPs have become the most clinically advanced nonviral vectors to deliver therapeutic nucleic acids of small interfering RNA (siRNA), messenger RNA (mRNA) or plasmid DNA (pDNA) as more than ten LNP–siRNA/mRNA/pDNA formulations have entered the stage of clinal trials [76-78]. LNP formulations for co-delivery of siRNA and mRNA have also been explored, which may enable the simultaneous knockdown of undesirable protein(s) and expression of desirable protein(s) [79]. Moreover, lipid-covered polymeric NPs and pure drug NPs have shown great benefits in drug delivery for their high efficiency and minor side effects [80, 81]. The batch methods to produce LNPs involve the stepwise mixing of the lipid-containing organic solution and the nucleic acid-containing aqueous solution to precipitate LNPs, which was generally achieved by extrusion or pipette mixing. The manufacturing challenge for batch methods lies in the poor control over the LNP properties, especially the LNP sizes of greater than 100 nm [79]. Microfluidic strategies have been applied to reduce LNP size and size dispersity, and improve the encapsulation efficiency of therapeutic reagents.

The microfluidic synthesis of LNPs, including the lipid-coated NPs, can be performed in different types of microfluidic mixers including SHM, HFF, 3D HFF with microvortices, and T-junction mixers. Producing LNPs using the SHM device has successfully overcome the main hurdle to the batch stepwise mixing of the high cost of the tens of milliliters of nucleic acid solution [44, 82]. **Figure 5A** shows the study that developed the SHM method for the synthesis of LNPs which managed to lower the requirement on the volume of input solutions from milliliter to microliter, thus saving expensive siRNA reagents [44]. As little as 10 μL of organic and aqueous solution was reliably mixed in milliseconds. Compared to the pipet mixing method which produced LNPs of ~ 180 nm in diameter, the SHM method decreased the LNP size below 100 nm. The LNP size was highly reproducible between repeated experiments and were further decreased to ~70 nm at the flow rates of 12 – 60 mL hr^{-1}. Moreover, the SHM method enabled the improvement of screening of lipid-like materials for siRNA delivery due to its rapid and small-scale manners. The crucial role of the size control of LNPs in siRNA delivery efficiency was shown by another study [45]. The large LNPs of 170 nm in diameter had poor gene silencing in vivo compared to the small LNP of 60 nm in diameter produced by the SHM method. The ability of SHM devices to precisely and reproducibly control the LNP size enabled researchers to further study the effect of LNP size on gene silencing by preparing siRNA-loaded LNPs of different sizes ranging from 27 to 117 nm [24]. It was found that 27 nm LNPs were unstable, and

117 nm LNPs failed to transport through liver vasculatures. The LNPs of 38 – 78 nm in diameter resulted in the most efficient hepatic gene silencing.

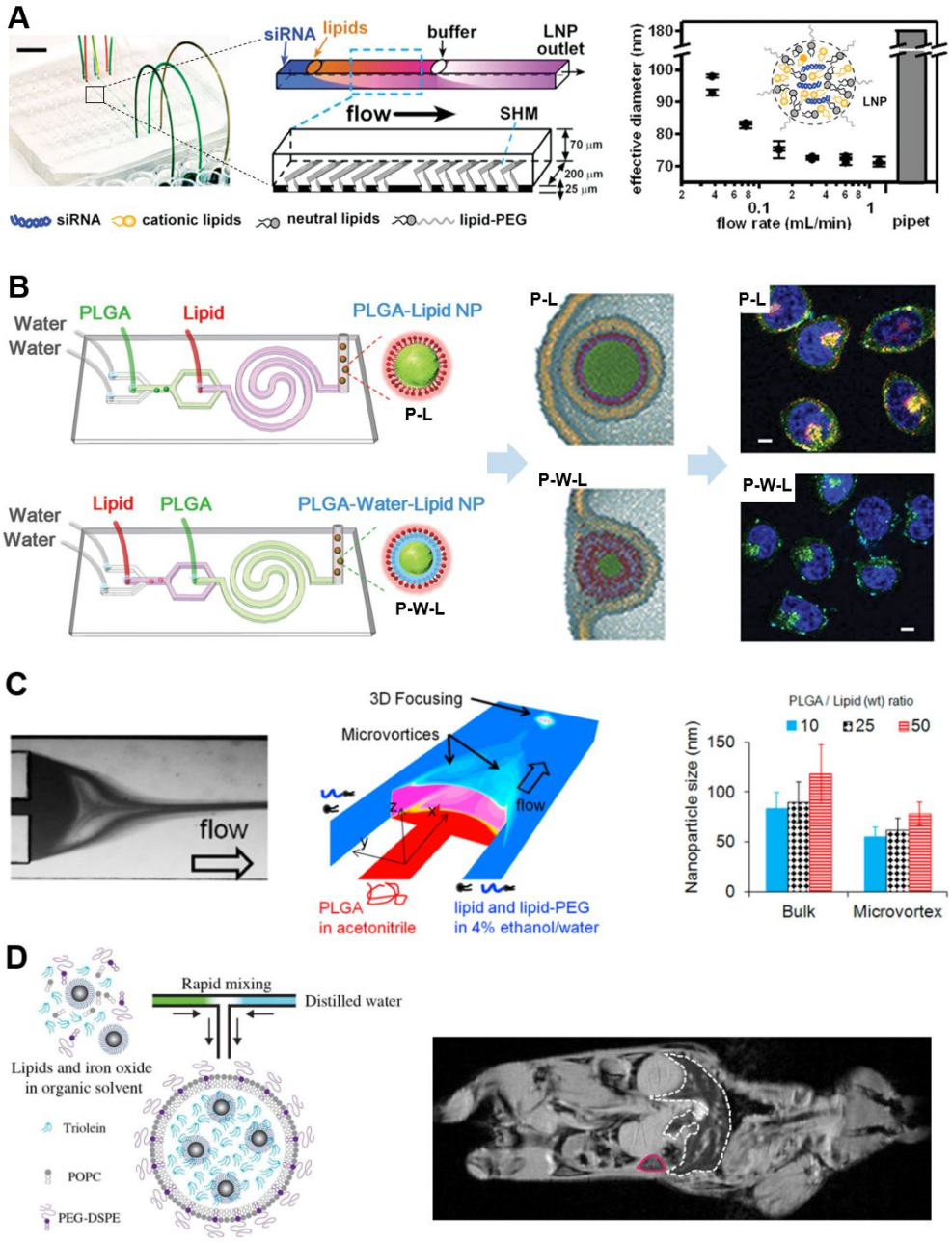

Figure 5. Microfluidic methods for the synthesis of lipid nanoparticles (LNPs). (A) Staggered herringbone micromixer (SHM). The LNP synthesis by SHM reduces the required volume of input solutions from milliliter to microliter, and decreases the particle size from approximately 180 to 70 nm. Reprinted with permission from ref. [44]. Copyright 2012 American Chemical Society. (B) Hydrodynamic flow focusing (HFF). A two-stage HFF device assembles NPs with a lipid shell – polymer core structure, and regulates the cellular uptake of NPs by their rigidity which leads to different dynamics of entry into the cell. Reprinted with permission from ref. [83]. Copyright 2014 Wiley.

(C) 3D HFF with microvortices. The 3D focusing by microvortices is generated at the Reynolds number of up to 150, fulfilling reduced particle size and PDI (55 – 80 nm, 0.1) compared to batch method (80 – 120 nm, 0.2). Reprinted with permission from ref. [53]. Copyright 2013 American Chemical Society. (D) T-junction mixer. The turbulent T-junction mixer operating at a high Reynolds number of 11,000 scales up the LNP production, and the encapsulation of iron oxide NPs into LNPs enhances the image contract for magnetic resonance imaging (MRI) of liver (dotted white line) and spleen (pink solid line). Reprinted with permission from ref. [50]. Copyright 2017 Royal Society of Chemistry.

As shown in **Figure 5B**, researchers used a two-stage HFF to assemble the NPs having a PLGA core/lipid shell structure [83]. The lipid shell could be monolayer (P-L) or bilayer (P-W-L) solely depending on injection order of PLGA and lipid solutions. The P-L and P-W-L NPs had different rigidity but the same composition, surface chemistry, and size. The cellular uptake of NPs was found to be regulated by rigidity. The rigid P-L NP was internalized smoothly, but the less rigid P-W-L NP significantly deformed during the internalization which impeded its entry into the cell. As a result, the HeLa cells took up more "hard" P-L NPs than the "soft" P-W-L NPs indicated by the higher fluorescence intensities of the cells incubated with the P-L NPs. **Figure 5C** shows the production of PLGA-lipid NPs with superior reproducibility and homogeneity using the 3D HFF device with microvortices [53]. The device operated at the Reynolds number of 30 – 150 yielding a high throughput up to 3 g hr^{-1}. The NP size was well controlled in the range of 55 – 80 nm with a small PDI of ~ 0.1. In comparison, the batch method produced larger NPs of 80 – 120 nm in diameter with a PDI of ~ 0.2. The production of LNPs can be conducted with the turbulent T-junction mixer at a high throughput (**Figure 5D**) [50]. The rapid mixing was induced by having two fluids flow directly toward each other with a perpendicular turbulent output, which required a high Reynolds number of 11,000. The size modulated over the range 35 – 150 nm was fulfilled by varying the flow and the core-to-surface lipid ratio. The encapsulation of iron oxide NPs into LNPs provided enhanced image contract for magnetic resonance imaging (MRI) of liver and spleen. The turbulent T-junction mixer offers an approach to scale up the LNP production; however, it may not be a preferred method for the applications such as high throughput screening of various LNP formulations since it cannot be scaled down to handle small volumes of the expensive reagents of nuclear acids or lipids.

3.3. Inorganic NPs

Inorganic NPs typically possess unique optical properties enabling them to respond to specific external stimuli including light, magnetic field, ultrasound, radiofrequency, and radiation, as well as internal stimuli such as pH, interstitial pressure, and conjugation of biomarkers [84-87]. Hence, inorganic NPs have been widely used as therapeutic, diagnostic, or imaging agents. Gold NPs

(AuNPs), having the unique surface plasmon resonance (SPR), are one of the most studied type among the inorganic NPs. Modulating the optical and photothermal properties of AuNPs has showing promising applications for clinical use such as tumor imaging [88], tumor ablation [89], and on-demand release of incorporated therapeutics [90]. Iron oxide NPs (IONPs) are another type of inorganic NPs which has been extensively investigated because of their uniqueness of innate magnetic responsiveness. IONPs are able to facilitate the combination of imaging with therapy, called theranostics, allowing for more precise drug delivery [91, 92]. IONPs can serve as therapeutic agents via magnetic hyperthermia in alternating magnetic field. The local increase in heat can be used to induce cancer cell death, as well as the triggered release of the loaded drug [93, 94]. Silica (SiO_2) NPs (SNPs) are also attractive for the drug delivery purpose as not only their size and shape, but also their porosity and chemical property of surface can be controlled, which gives them the ability to store and release both hydrophilic and hydrophobic drugs [95-97]. Inorganic NPs are commonly produced by chemical methods (such as chemical reduction) to induce the NP precipitation. The batch methods face significant challenges to scale up the production. The batch methods are not able to separate the nanoprecipitation stages of nucleation and growth leading to the problem of high levels of batch-to-batch variation of NP size.

The microfluidic devices such as micro-droplet generator, glass capillary, and T-junction mixer have been developed for the synthesis or surface modification of inorganic NPs. **Figure 6A** shows one study using the micro-droplet generator to synthesize silver NPs [98]. The silver salt (silver nitrate) solution was flow focused with the other aqueous solution containing the reducing agent of tannic acid and the stabilizing agent of trisodium citrate forming a series of micro-droplets. The droplet volume could be modulated within 30 – 80 picoliters by varying the input flow rates. The experiment result in Figure 6A exhibits the mixing inside droplets via the observation of the fluorescence of the tracer of rhodamine B. The mixing efficiency of 85% was achieved within 40 ms, which was considered fast enough for precipitation reaction and NP formation. Another study utilizing the micro-droplet generator to synthesize silver and gold NPs is shown in **Figure 6B** [99, 100]. The micro-droplets were generated by a T junction. The droplet contained the ionic liquid solutions of the metal salt precursor and the reductant. The gold NPs synthesized by the micro-droplet method was 29% smaller than the batch method. More striking differences were observed for silver NPs which had a well-defined spherical shape in the microfluidic synthesis but appeared as large coral-like assemblies in the batch synthesis.

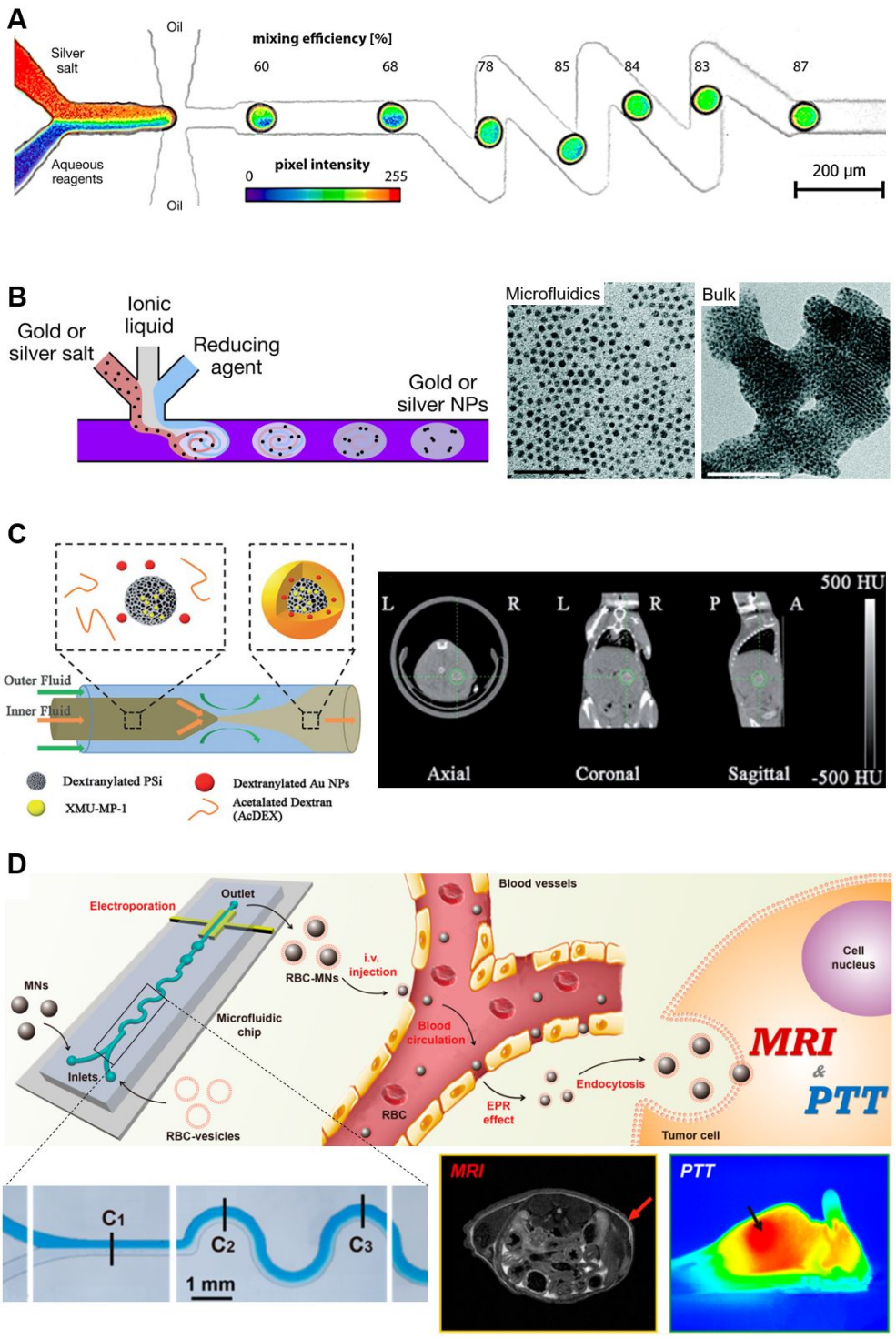

Figure 6. Microfluidic methods for the synthesis and surface modification of inorganic NPs. (A) Micro-droplet generator (by flow focusing). Efficiency of the in-droplet mixing between silver salt and reducing reagent reaches 85% within 40 ms for homogeneous precipitation reaction and silver NP formation. Reprinted with permission from ref. [98]. Copyright 2019 Springer. (B) Micro-droplet generator (by T junction). The gold NPs are generated in the micro-droplets with a well-defined spherical shape and 29% smaller than batch method. Reprinted with permission from refs. [99, 100].

Copyright 2012 American Chemical Society. Copyright 2021 Elsevier. (C) Glass capillary. Surface modification of silicon NPs with a polymer matrix is conducted in a glass capillary device, and this microfluidically-synthesized nanohybrid serves as a theranostic reagent with increased local drug concentration in the lesion area of liver. Reprinted with permission from ref. [101]. Copyright 2017 Wiley. (D) T-junction mixer. The utilization of U-shaped turns after the T-junction enhances the mixing between iron oxide NPs and the surface modification material of blood cell membrane-derived vesicles, and the core-shell nanohybrid exhibits enhanced efficiency of tumor magnetic resonance imaging (MRI) and photothermal therapy (PTT). Reprinted with permission from ref. [102]. Copyright 2017 American Chemical Society.

The study in **Figure 6C** used the microfluidic glass capillary device to conduct the surface modification of silicon NPs with a polymer matrix [101]. Both the silicon and gold NPs were encapsulated in the polymer matrix by alternating the NPs' surface properties. The therapeutic compound of XMU-MP-1 was also loaded to the porous silicon NPs via the nanoprecipitation in the glass capillary. This nanohybrid showed potential as a theranostic reagent for the disease of acute liver failure (ALF). The microfluidic synthesized NPs increased the local drug concentration in the lesion area of liver and enhanced the CT signal to generate a distinguishable area in CT images by the accumulation of NPs in the mice with ALF disease. **Figure 6D** shows a study creating the biomimetic cell membrane-coated NPs via the surface modification of iron oxide NPs (IONPs) [102]. The microfluidic mixing between the IONPs and the blood cell membrane-derived vesicles (RBC vesicles) were fulfilled using a variant of T-junction mixer involving a series of U-shaped turns followed by an electroporation zone. The two reagents were observed to be evenly mixed after the third U turn. This core-shell nano-formulation of RBC-IONP had the magnetic and photothermal properties because of the IONP core, and the long blood circulation characteristic owing to the RBC shell. Thus, the RBC-IONPs were used for enhanced tumor magnetic resonance imaging (MRI) and photothermal therapy (PTT) while the microfluidically-prepared NPs showed significantly better treatment effect than batch-prepared NPs.

3.4. Drug nanocrystals

Nowadays, a large portion of drugs are designed and generated as poorly water-soluble molecules which results in the majority of the failures in new drug development [103, 104]. Specifically, more than 40% of the drugs are classified as low solubility drugs by the biopharmaceutics classification system (BCS) [105], and approximately 70 – 90% of new drugs have the problem of poor aqueous solubility [106]. The incorporation of hydrophobic drugs into NPs enables faster dissolution rate and higher saturation concentration of the drugs in aqueous solutions [107, 108]. Thus, as a drug carrier, NPs improve the solubility and bioavailability of the encapsulated drugs. The bioactivity and stability of the encapsulated drugs can also be enhanced by the NP's protection from rapid metabolism and

clearance [109, 110]. Moreover, the nano-formulation can contribute to less toxicity and improved therapeutic efficacy of a drug via spatiotemporal control of drug release [111-114].

Drug nanocrystals, or called pure drug NPs, are a versatile tool for the delivery of the hydrophobic drugs as a simple core-shell nanostructure. The drug nanocore is formed first, and then encapsulated by a shell/layer of stabilizer. Polymers and surface-active agents are the most commonly used stabilizers for pharmaceutical nanocrystals. Stabilizers influence not only the stability but also the bioavailability of nanocrystals. For example, Pluronic-grafted chitosan copolymer, as the stabilizer of paclitaxel (PTX) nanocrystals, improved the relative bioavailability of PTX by 12.6 folds compared to Taxol™ [115]. Among the various nano-formulations, the advantages of drug nanocrystals include high drug loading, low preparation cost, and flexible administration routes [116]. Drug nanocrystals are referred to as nanosuspension when they are suspended in aqueous medium [104]. Apart from their conventional clinical or preclinical use of oral delivery of hydrophobic drugs, drug nanocrystals can be more broadly used via other administration routes of transdermal, pulmonary, opththalmic, buccal, and intravenous [117-120].

The top-down milling method is not possible or require a very long process to reduce the size of drug nanocrystals below 100 nm. For example, using the media milling technique, the fenofibrate nanocrystals with the stabilizer of Soluplus® and HPMC, respectively, were produced with sizes of 344 nm and 642 nm, respectively [121]. The bottom-up microfluidic nanoprecipitation method can help to reduce the size of drug nanocrystals. **Figure 7A** shows a commonly used microfluidic device of Y-junction mixer to synthesize hydrocortisone nanosuspension. The ethanolic drug solution was mixed with the aqueous solution containing stabilizers and then introduced to a bulk solution of phosphate buffered saline (PBS) with stabilizers under continuous sonication. A hydrocortisone nanosuspension with a mean size of 295 ± 32 nm was generated which was comparable to the minimum size of hydrocortisone nanocrystals produced by the wet milling method (milling time up to 105 minutes). The Y-junction mixer was also adopted in other studies to synthesize of the nanocrystals of different hydrophobic drugs of danazol [122], cefuroxime axetil [123], and atorvastatin calcium [124]. These drug nanocrystals produced by Y-junction mixers were generally larger than 300 nm in size. The drug nanocrystal of rubrene was prepared smaller than 100 nm with a HFF device shown in **Figure 7B** [125]. The ethanolic rubrene solution was focused in the HFF configuration by the stabilizer-containing aqueous flows. The efficient diffusion in the region of the focused drug-containing stream was confirmed by confocal fluorescence microscopy in the presence of fluorescein. The rubrene nanocrystals of 50 – 110 nm in mean diameter were produced by the HFF device by controlling the aqueous-to-organic flow ratio. The nanocrystals of paclitaxel (PTX) and sorafenib (SFN) stabilized by the coating polymer of hypromellose acetate succinate (HF) were generated with the

controlled size of 60 − 450 nm and 70 − 550 nm, respectively, in a study utilizing the glass capillary device for the drug nanocrystal synthesis (**Figure 7C**) [126]. To reduce the nanocrystal size below 100 nm, a high Reynold number of Re > 500 was required. A droplet-based microfluidic approach was also proposed to synthesize the drug nanocrystal of curcumin [127]. As shown in **Figure 7D**, the ethanolic curcumin solution was mixed with the aqueous solution containing stabilizers in a T-junction mixer, and then formed hanging droplets out of the micro-channel in the open-air environment. The simultaneous mixing was activated by the inherent chaotic advection within each droplet, which was observed via the planar laser-induced fluorescence. As a result, curcumin nanocrystals of 190 − 450 nm in mean diameter were generated by this droplet-based method depending on the concentration of curcumin.

Surface stabilizer is necessary for the drug nanocrystal stabilization; however, grafting the ligands to the surface of nanocrystals which are made of pure drug molecules is technically challenging due to lack of functional chemical groups. **Figure 7E** shows the combination of ionic surfactants and polymeric stabilizers for drug nanocrystal stabilization, which utilize the ionic surfactants for electrostatic repulsion and the polymeric stabilizers for steric hindrance [104]. A recently employed coating material of metal-phenolic networks (MPNs) for drug nanocrystal stabilization is shown is **Figure 7F** [128]. MPNs are supramolecular structures formed by the rapid coordination of natural polyphenols (such as tannic acid (TA), garlic acid (GA), and epigallocatechin gallate (EGCG)) with metal ions (such as Fe^{3+}, Al^{3+}, Sr^{2+}, and Cu^{2+}) [129, 130]. MPNs are flexible and compatible with other biomaterials, so they have been developed for the delivery of imaging and therapeutic agents [129, 131-135]. MPNs are also non-cytotoxic and degradable making them attractive to encapsulate proteinosomes, microbes, and mammalian cells [136-138]. Recently, MPNs have been employed as a coating material for drug nanocrystal stabilization. As a thin shell, MPNs can achieve high drug loading; moreover, MPNs can provide a functionalized surface for the nanocrystal to graft other ligands [128, 139, 140]. MPN-coated nanocrystals have been produced by batch nanoprecipitation methods for the hydrophobic drugs of paclitaxel [128], carfilzomib [139], vitamin D [140], curcumin [141], rapamycin [142], chlorin e6 [143], SN-38 [144], simvastatin [145], andrographolide [145], and cabazitaxel [146]. The batch methods involve manual pipet mixing and the postprocessing step of sonication which makes it time-consuming and labor-intensive work to scale from benchtop production to larger volume batches. Lately, our group developed a microfluidic HFF method for the synthesis of MPN-coated nanocrystals of hydrophobic drugs [39]. As shown in **Figure 7G**, the mechanism of encapsulating of a variety of hydrophobic drugs is established based on the time scales of microfluidic mixing and drug nucleation. The microfluidically-synthesized MPN-coated nanocrystals of vitamin D, curcumin, and paclitaxel had well-controlled sizes of 80 – 200 nm, high drug loadings of 40 – 70%, and a throughput of up to 70 mg hr^{-1} per channel exhibiting scale-up potential.

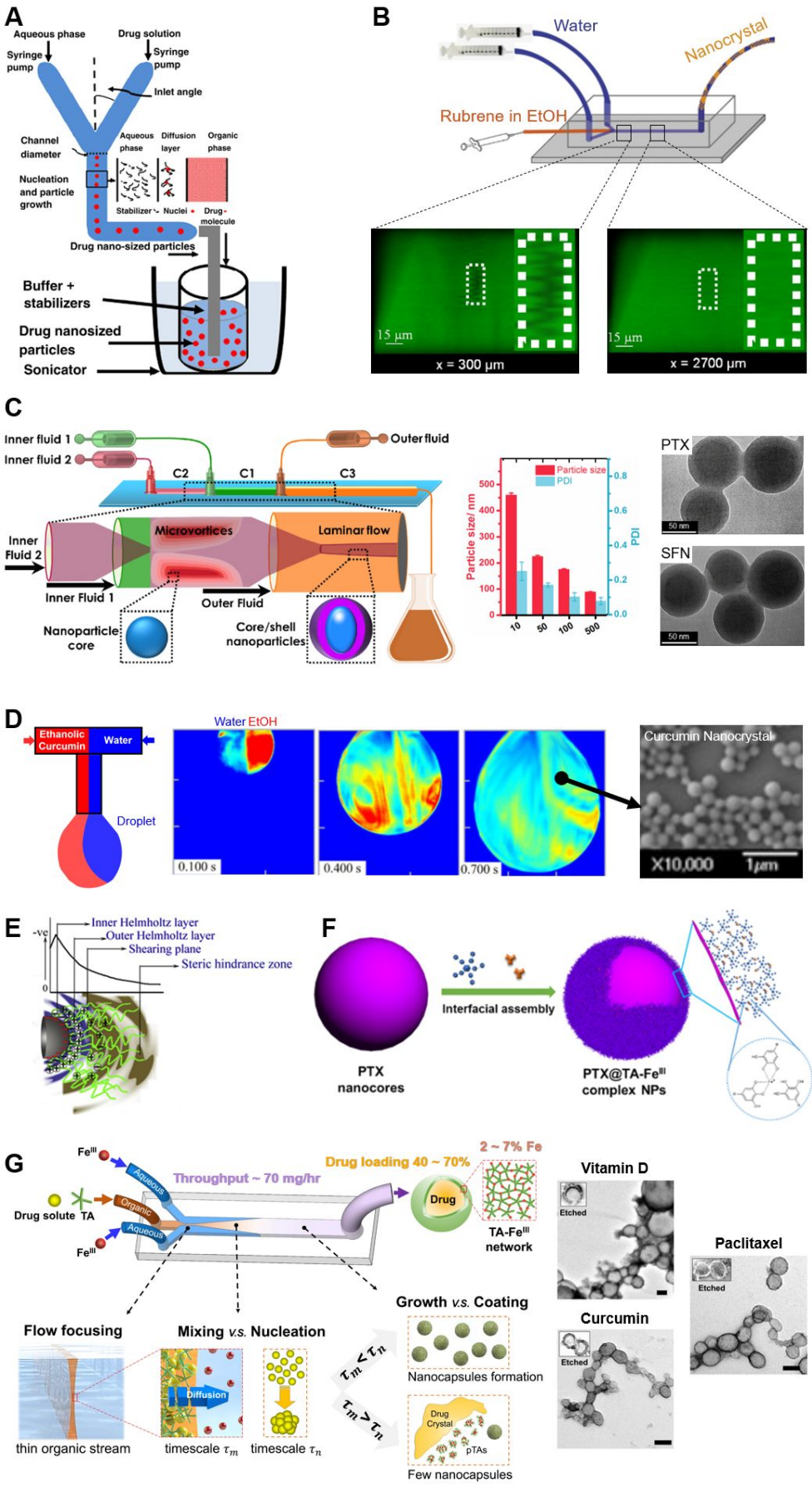
A
Aqueous phase
Drug solution
Syringe pump
Syringe pump
Inlet angle
Channel diameter
Aqueous phase
Diffusion layer
Organic phase
Nucleation and particle growth
Stabilizer
Nuclei
Drug molecule
Drug nano-sized particles
Buffer + stabilizers
Drug nanosized particles
Sonicator
B
Water
Nanocrystal
Rubrene in EtOH
15 μm
x = 300 μm
15 μm
x = 2700 μm
C
Inner fluid 1
Inner fluid 2
Outer fluid
C2
C1
C3
Inner Fluid 2
Microvortices
Laminar flow
Inner Fluid 1
Outer Fluid
Nanoparticle core
Core/shell nanoparticles
Particle size
PDI
Particle size/ nm
PDI
PTX
50 nm
SFN
50 nm
D
Ethanolic Curcumin
Water
Droplet
Water EtOH
0.100 s
0.400 s
0.700 s
Curcumin Nanocrystal
X10,000
1μm
E
Inner Helmholtz layer
Outer Helmholtz layer
Shearing plane
Steric hindrance zone
-ve
0
F
Interfacial assembly
PTX nanocores
PTX@TA-Fe^{III} complex NPs
G
Fe^{III}
Aqueous
Organic
Aqueous
Drug solute TA
Fe^{III}
Throughput ~ 70 mg/hr
Drug loading 40 ~ 70%
2 ~ 7% Fe
Drug
TA-Fe^{III} network
Vitamin D
Etched
Paclitaxel
Etched
Curcumin
Etched
Flow focusing
Mixing v.s. Nucleation
Growth v.s. Coating
Diffusion
$\tau_m < \tau_n$
$\tau_m > \tau_n$
Nanocapsules formation
Drug Crystal
pTAs
Few nanocapsules
thin organic stream
timescale τ_m
timescale τ_n

Figure 7. Microfluidic methods for the synthesis of drug nanocrystals (pure drug NPs). (A) Y-junction mixer. As the simplest bottom-up microfluidic nanoprecipitation method, the Y-junction mixer with the aid of sonication can produce nanocrystals of the hydrophobic drug of hydrocortisone with the diameter of ~ 300 nm. Reprinted with permission from ref. [147]. Copyright 2011 Elsevier. (B) Hydrodynamic flow focusing (HFF). The 3D flow focusing device enables fast diffusion of the central stream and thus generates rubrene nanocrystals smaller than 100 nm. Reprinted with permission from ref. [125]. Copyright 2010 Elsevier. (C) Glass capillary. The nanocrystals of paclitaxel (PTX) and sorafenib (SFN) smaller than 100 nm are synthesized at the conditions of Re > 500. Reprinted with permission from ref. [126]. Copyright 2017 American Chemical Society. (D) T-junction mixer followed by inner-droplet mixing. The mixing by the inherent chaotic advection within the hanging droplet enables the production of curcumin nanocrystals smaller than 200 nm. Reprinted with permission from ref. [127]. Copyright 2010 Springer. (E) Combined with the electrostatic repulsion provided by ionic surfactants, polymer molecules serve as the surface stabilizer for the drug nanocrystal stabilization by providing additional steric hindrance zone. Reprinted with permission from ref. [104]. Copyright 2013 Elsevier. (F) Metal-phenolic (Fe^{3+}-tannic acid (TA)) network (MPN) as a stabilizer for the drug nanocrystal of PTX. Reprinted with permission from ref. [128]. Copyright 2016 American Chemical Society. (G) A timescale-guided microfluidic HFF method for the synthesis of MPN-coated nanocrystals of different hydrophobic drugs of PTX, vitamin D, and curcumin. Reprinted with permission from ref. [39]. Copyright 2023 Elsevier.

Surface stabilizer is necessary for the drug nanocrystal stabilization; however, grafting the ligands to the surface of nanocrystals which are made of pure drug molecules is technically challenging due to lack of functional chemical groups. **Figure 7E** shows the combination of ionic surfactants and polymeric stabilizers for drug nanocrystal stabilization, which utilize the ionic surfactants for electrostatic repulsion and the polymeric stabilizers for steric hindrance [104]. A recently employed coating material of metal-phenolic networks (MPNs) for drug nanocrystal stabilization is shown is **Figure 7F** [128]. MPNs are supramolecular structures formed by the rapid coordination of natural polyphenols (such as tannic acid (TA), garlic acid (GA), and epigallocatechin gallate (EGCG)) with metal ions (such as Fe^{3+}, Al^{3+}, Sr^{2+}, and Cu^{2+}) [129, 130]. MPNs are flexible and compatible with other biomaterials, so they have been developed for the delivery of imaging and therapeutic agents [129, 131-135]. MPNs are also non-cytotoxic and degradable making them attractive to encapsulate proteinosomes, microbes, and mammalian cells [136-138]. Recently, MPNs have been employed as a coating material for drug nanocrystal stabilization. As a thin shell, MPNs can achieve high drug loading; moreover, MPNs can provide a functionalized surface for the nanocrystal to graft other ligands [128, 139, 140]. MPN-coated nanocrystals have been produced by batch nanoprecipitation methods for the hydrophobic drugs of paclitaxel [128], carfilzomib [139], vitamin D [140], curcumin

[141], rapamycin [142], chlorin e6 [143], SN-38 [144], simvastatin [145], andrographolide [145], and cabazitaxel [146]. The batch methods involve manual pipet mixing and the postprocessing step of sonication which makes it time-consuming and labor-intensive work to scale from benchtop production to larger volume batches. Lately, our group developed a microfluidic HFF method for the synthesis of MPN-coated nanocrystals of hydrophobic drugs [39]. As shown in **Figure 7G**, the mechanism of encapsulating of a variety of hydrophobic drugs is established based on the time scales of microfluidic mixing and drug nucleation. The microfluidically-synthesized MPN-coated nanocrystals of vitamin D, curcumin, and paclitaxel had well-controlled sizes of 80 – 200 nm, high drug loadings of 40 – 70%, and a throughput of up to 70 mg hr^{-1} per channel exhibiting scale-up potential.

3.5. Microfluidic separation and purification of nano drugs and biologics

In recent decades, microfluidic techniques have advanced to manipulate nanoscale bioparticles, including trapping [148, 149], focusing [150, 151] and separation [152] using various forces such as acoustic radiation force [153], elastic lift force [154], dielectrophoresis force [155-157] as well as inertial and viscous forces [158]. The fluid properties are relevant to particle separation, such as viscosity (resistance to flow), density, and fluid velocity. Laminar flow (Re << 2000) not only occurs but also a Stokes flow (Re << 1) in the microfluidic channel. Particles in a flow experience shear and normal stresses, generating parallel forces (drag force) and perpendicular forces (wall effect and shear gradient lift forces) to the main flow direction and are aligned in the equilibrium position in **Figure 8A** [159]. Drag forces generally accelerate particles until they reach flow speed equilibrium [160]. In passive separation technologies, particles are controlled by hydrodynamic flow in microfluidics, while active separation technologies involve external forces such as magnetic, acoustic, optical, or electrical effects, often necessitating additional microchannel equipment [161]. In active separation technologies, particle behaviors are intricately governed by external forces. For instance, as depicted in **Figure 8B**, the particle movement is controlled by a magnetic force [162]. When a particle is suspended within a uniform electric field, its movement is significantly influenced by the gradients within a non-uniform electric field, ultimately resulting in a net force (**Figure 8C**) [163]. Furthermore, the surface acoustic wave (SAWs) are generated by the transducer called an interdigital transducers (IDTs) and particle movements are affected by SAWs as shown in **Figure 8D** [164]. The separation and purification of nano drugs and biologics, such as liposomes, viruses, DNA nano-balls, and extracellular vesicles (EVs), are essential prerequisites for their biomedical and clinical applications [165-168]. Both passive and active techniques including acoustofluidics [169-171], hydrodynamics [172-174], and dielectrophoresis (DEP) [175-179] have been employed for the separation and purification of these substances.

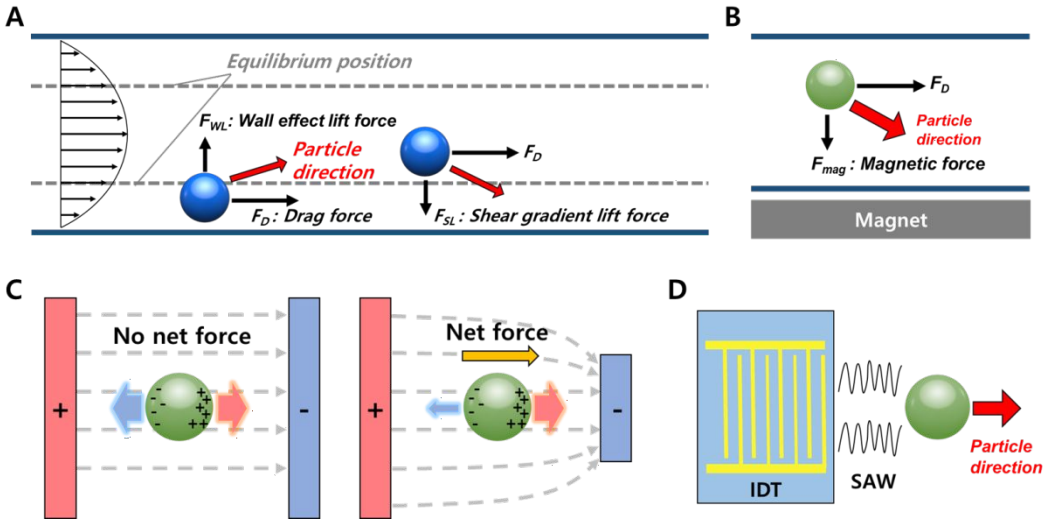

Figure 8. Particle separation technologies. (A) Hydrodynamic force. Particles move to the equilibrium position and are aligned by parallel forces (drag force) and perpendicular forces (wall effect and shear gradient lift forces). (B) Magnetic force. The direction of particle movement is controlled by a magnetic force, pulling the particles towards the magnet. (C) Electric force. The gradients of a non-uniform electric field lead to a net force and thus control the movement of a suspended particle. (D) Acoustic force. The interdigital transducers (IDTs) generate surface acoustic waves (SAWs) to modulate the particle motion.

Acoustofluidic technologies make use of acoustic waves to precisely control fluids and particles immersed in fluids, which enables contact-free and biocompatible separation of NPs. Particles containing liquid are given motion by the created density, velocity, or pressure field as a result of the acoustic waves propagating in liquid. The transducer utilized for surface acoustic wave (SAWs) generation and reception are called interdigital transducers (IDTs). **Figure 9A** shows the design of stereo acoustic stream (SteAS) for NP separation [169]. A droplet is placed on a PDMS ring located in between of two IDTs. The SteAS makes the droplet start to spin as the surface acoustic waves (SAWs) propagate into the droplet. Then the particles within the spinning droplet migrate toward its center, following a dual-axis rotational trajectory. The SteAS was able to capture 30-nm polystyrene NPs and continuously focus 150-nm polystyrene NPs. This acoustofluidic technology enables the enrichment and continuous size-based separation of NPs, and thus holds potential for applications in analytical chemistry and nano-drugs.

The hydrodynamics method for NP separation can utilize viscoelastic microfluidics to manipulate NPs in a more precise manner than the inertial microfluidics [172, 173]. Viscoelasticity-induced microfluidic devices have been utilized to focus and separate particles. **Figure 9B** shows a design of viscoelastic microfluidics mediated with λ-DNA and aptamer, by which EV subpopulations were size-selectively

separated [173]. The cell-derived EVs include exosomes (EXOs), microvesicles (MVs), and apoptotic bodies (ABs), which can utilize aptamers specific to HER2 and EpCAM. EXOs with sizes below 200 nm were submerged in the viscoelastic sample fluid, experiencing the centerline-directed elastic lift force. Conversely, MVs and ABs with sizes equal to or exceeding 200 nm were repelled by the force exerted by the flow, leading them to migrate towards the Newtonian sheath stream devoid of elasticity. Thus, these three EV subpopulations were separated for surface protein analysis of individual EVs. The panel of aptamers for the multiple detection of EV markers can be expanded, and the diagnostic value of EV subpopulations for different types of cancers can be further studied using this viscoelastic microfluidics.

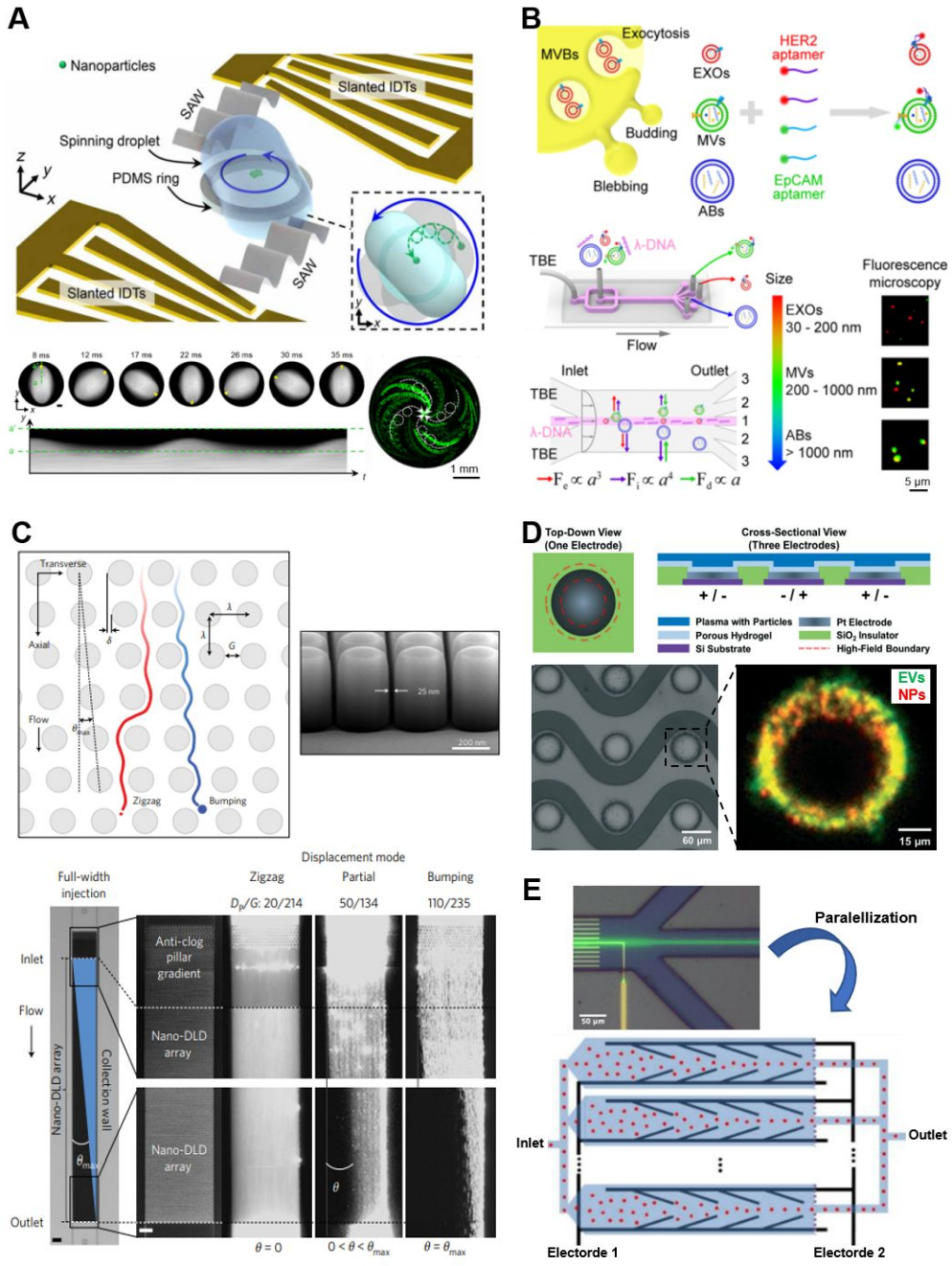

Figure 9. Microfluidic strategies for separation and purification of nano-sized particles. (A) Acoustofluidics. Operational principles of an acoustofluidic centrifuge platform and dynamics of droplet spinning and particle manipulation within droplet. Reprinted with permission from ref. [169]. (B) Viscoelastic hydrodynamics. Process of size-selective separation of extracellular vesicle (EV) subpopulations through implementation of λ-DNA mediated viscoelastic microfluidics. Reprinted with permission from ref. [173]. Copyright 2019 American Chemical Society. (C) Nanoscale deterministic lateral displacement (nano-DLD) arrays for NP separation. Reprinted with permission from ref. [152]. Copyright 2016 Springer. (D) Dielectrophoresis (DEP) for stagnant fluids. An example shows the collection of polystyrene NPs (red) and EVs (green) by DEP arrays. Reprinted with permission from ref. [177]. Copyright 2021 American Chemical Society. (E) DEP for continuous flows. Sub-100 nm polymer particles (green) focused in the center of channel, as well as the parallelization design. Reprinted with permission from ref. [176].

The hydrodynamics method of deterministic lateral displacement (DLD) employs pillar arrays to continuously separate particles based on their size. The pillar arrays induce fluid bifurcation and result in a distinctive number of streamlines within the gaps. Particles that are smaller than the critical diameter follow the streamlines in the Zigzag mode (migration angle $\theta = \theta_{max}$), otherwise the particles behave differently in the Bumping mode ($\theta = 0$), or the mode of Partial displacement ($0< \theta < \theta_{max}$) [180]. **Figure 9C** shows a design of nanoscale deterministic lateral displacement (nano-DLD) arrays with consistent gap sizes ranging from 25 to 235 nm [152]. These nano-DLD arrays effectively separated particles within the size range of 20 to 110 nm with sharp resolution. This hydrodynamics method of nano-DLD allows continuous and rapid NP sorting with a single-particle resolution without the need of particle labelling. The on-chip sorting and quantification of biocolloids, such as EVs, can also be fulfilled using the DLD technique.

Dielectrophoresis (DEP) refers to the movement of an object caused by the influence of DEP forces; specifically, when an object is suspended in a fluid and exposed to a non-uniform electric field, the contrasting dielectric properties between the object and its surrounding medium result in the generation of DEP forces acting on the object [175, 181, 182]. **Figure 9D** shows the measurement of fluorescence intensity of EVs from blood plasma (green) and polystyrene NPs (blue) captured on the surface of DEP regions within a microfluidic device [177]. This optical DEP technique can be adapted to other lab-on-a-chip platforms that feature analysis of cancer-related biomarkers. **Figure 9E** shows another example of DEP microfluidics achieving the upconcentration and sorting of NPs in a continuous flow. The sub-100 nm particles (green fluorescence) were focused towards the center of the channel and directed towards the center outlet by the DEP force from a DC field. For the parallelization of channels utilizing the DEP force from an AC field, the inclined microsized electrodes

in a zig-zag three-tooth pattern was found to generate the largest DEP force to focus the NPs with a diameter of 84 or 47 nm. The massive parallelization of this DEP microfluidics can increase the throughput by a factor of 1250, which shows the potential for the applications for the purposes of clinical diagnosis and nano-drug purification.

4. Summary

The success of microfluidic techniques in dealing with the batch-to-batch variations of the batch synthesis methods for nano-formulations relies on the small scale of the microfluidic mixing which makes the precises control of the rapid diffusive mass transfer possible. The micrometer scale of microfluidics enables short mixing time, as well as uniform mixing flow patterns, yielding the small size and narrow size distribution of the microfluidically synthesized NPs. However, scaling up the microfluidic throughput to the industrial level is challenging. It is notable that the microfluidic flow capacity, *Q*, dramatically decreases with the decrease of channel size, *h*, due to the increase of hydraulic resistance, R_H, which can be expressed as $Q \propto {R_H}^{-1} \propto h^4$ [33]. For example, the flow capacity may be 80 times higher with a 3 times larger microfluidic channel (e.g. 300 μm *versus* 100 μm). Thus, although the continuous-flow manner makes the microfluidic techniques promising for large-scale production, it would be still meaningful to estimate the maximum microfluidic channel size for the synthesis of nano-formulations, guided by the timescale-based mechanism of mixing time versus precipitation time during the nanoprecipitation process.

Microfluidic channels can be fabricated out of a variety of materials such as polymers, glass, and silicon. Polymers are currently the most promising materials for microfluidic devices due to the advantages of flexibility, versatility, and biocompatibility, among which polydimethylsiloxane (PDMS) is undoubtedly the most widely used material [183-185]. Efforts are also made on the development of alternative materials beyond PDMS, such as non-binding polymers or plastics, due to PDMS's non-specific adsorption of proteins and other small molecule drugs [186-189]. The microchannel geometry can be fabricated by soft lithography and other lithography techniques such as reactive-ion etching, electron-beam lithography, and direct laser writing [190-193]. Fabrication of microfluidic devices can also be conducted by 3D printing or laser cutting as potential approaches for commercialization [194, 195]. However, the high entry level due to the knowledge requirement for fluid dynamics, and the complex configurations of microfluidics to fabricate, are still hindering the utilization of microfluidics by broader research and industrial communities.

Despite the challenges discussed above, the development of microfluidics is rapidly evolving to solve the current problems and expand to future directions. For example, one of the main issue of channel clogging is being addressed by 3D HFF and glass capillary techniques, and the throughput scaling

up to the industrial level is promising to be fulfilled by the parallelization of microfluidic devices [196, 197]. For future directions, the development of integrated microfluidic synthesis and separation devices with in-line characterization and control set-ups [198] is highly desirable, as it would allow real-time monitoring and in-process adjustment to optimize the production quality of nano-formulations. Microfluidics can also be a modular manufacturing technology for the future decentralized approach to nanomedicine manufacturing, which may facilitate the design and production of nanomedicine to meet the local or individual needs; for example, the development of microfluidics may be able to deal with the strained mRNA-LNP production which caused shortages of the vaccine [199]. For now, the microfluidic technique is more developed in the scenario of NP synthesis, while the drug delivery evaluation on the synthesized nano-formulation requires new developments of platforms or techniques for nanomedicine. Many nano-formulations showed satisfactory delivery in vitro, but failed when it came to the in vivo environments [200-202]. One main challenge in the drug delivery evolution is the modular platform that maintains necessary physicochemical properties which the conventional 2D monolayer cell culture system can not provide [203-205]. The combination of the microfluidic techniques of NP synthesis platform, as well as the NP delivery evaluation platform such as the tumor-on-a-chip models of pancreatic cancer and breast cancer developed in our lab [206-209], can play an important role in the pre-clinical phase trials for nanoparticle-based drug formulation development.

ACKNOWLEDGEMENTS

This study was partially supported by grants from NIH (R01 CA254110 and U01 CA274304), NSF (MCB-2134603) and the Purdue University Institute for Cancer Research (P30 CA023168), and a Program Grant from Purdue Institute for Drug Discovery.

REFERENCES

[1] M. Germain, F. Caputo, S. Metcalfe, G. Tosi, K. Spring, A.K.O. Åslund, A. Pottier, R. Schiffelers, A. Ceccaldi, R. Schmid, Delivering the power of nanomedicine to patients today, Journal of Controlled Release, 326 (2020) 164-171.
[2] R. van der Meel, E. Sulheim, Y. Shi, F. Kiessling, W.J.M. Mulder, T. Lammers, Smart cancer nanomedicine, Nature nanotechnology, 14 (2019) 1007-1017.
[3] I. de Lázaro, D.J. Mooney, Obstacles and opportunities in a forward vision for cancer nanomedicine, Nature materials, 20 (2021) 1469-1479.
[4] S.J. Shepherd, D. Issadore, M.J. Mitchell, Microfluidic formulation of nanoparticles for biomedical applications, Biomaterials, 274 (2021) 120826.
[5] S. Bisso, J.-C. Leroux, Nanopharmaceuticals: A focus on their clinical translatability, International journal of pharmaceutics, 578 (2020) 119098.
[6] L.A. Jackson, E.J. Anderson, N.G. Rouphael, P.C. Roberts, M. Makhene, R.N. Coler, M.P. McCullough, J.D. Chappell, M.R. Denison, L.J. Stevens, An mRNA vaccine against SARS-CoV-2—preliminary report, New England journal of medicine, 383 (2020) 1920-1931.
[7] L. Milane, M. Amiji, Clinical approval of nanotechnology-based SARS-CoV-2 mRNA vaccines: impact on translational nanomedicine, Drug delivery and translational research, 11 (2021) 1309-1315.
[8] J.S. Thomas, D. Habib, D.L. Hanna, I. Kang, S. Iqbal, J.J. Nieva, D. Tsao-Wei, F. Acosta, M. Hsieh, Y. Zhang, A phase 1 trial of FID-007, a novel nanoparticle paclitaxel formulation, in patients with solid tumors, in, Wolters Kluwer Health, 2021.
[9] Z.A. Wainberg, H.S. Hochster, E.J. Kim, B. George, A. Kaylan, E.G. Chiorean, D.M. Waterhouse, M. Guiterrez, A. Parikh, R. Jain, Open-label, phase I study of nivolumab combined with nab-paclitaxel plus gemcitabine in advanced pancreatic cancer, Clinical Cancer Research, 26 (2020) 4814-4822.
[10] S.M. Stavis, J.A. Fagan, M. Stopa, J.A. Liddle, Nanoparticle manufacturing–heterogeneity through processes to products, ACS Applied Nano Materials, 1 (2018) 4358-4385.
[11] S. Mülhopt, S. Diabaté, M. Dilger, C. Adelhelm, C. Anderlohr, T. Bergfeldt, J. Gómez de la Torre, Y. Jiang, E. Valsami-Jones, D. Langevin, Characterization of nanoparticle batch-to-batch variability, Nanomaterials, 8 (2018) 311.
[12] A. Zielińska, F. Carreiró, A.M. Oliveira, A. Neves, B. Pires, D.N. Venkatesh, A. Durazzo, M. Lucarini, P. Eder, A.M. Silva, Polymeric nanoparticles: production, characterization, toxicology and ecotoxicology, Molecules, 25 (2020) 3731.
[13] S. Bohrey, V. Chourasiya, A. Pandey, Polymeric nanoparticles containing diazepam: preparation, optimization, characterization, in-vitro drug release and release kinetic study, Nano Convergence, 3 (2016) 1-7.
[14] Y. Yang, Y. Ding, B. Fan, Y. Wang, Z. Mao, W. Wang, J. Wu, Inflammation-targeting polymeric nanoparticles deliver sparfloxacin and tacrolimus for combating acute lung sepsis, Journal of Controlled Release, 321 (2020) 463-474.
[15] S.C. Semple, A. Akinc, J. Chen, A.P. Sandhu, B.L. Mui, C.K. Cho, D.W.Y. Sah, D. Stebbing, E.J. Crosley, E. Yaworski, Rational design of cationic lipids for siRNA delivery, Nature biotechnology, 28 (2010) 172-176.
[16] A. Bagde, K. Patel, S. Kutlehria, N. Chowdhury, M. Singh, Formulation of topical ibuprofen solid lipid nanoparticle (SLN) gel using hot melt extrusion technique (HME) and determining its anti-inflammatory strength, Drug delivery and translational research, 9 (2019) 816-827.
[17] J. Hu, W.K. Ng, Y. Dong, S. Shen, R.B.H. Tan, Continuous and scalable process for water-redispersible nanoformulation of poorly aqueous soluble APIs by antisolvent precipitation and spray-drying, International journal of pharmaceutics, 404 (2011) 198-204.
[18] Y. Lu, Y. Li, W. Wu, Injected nanocrystals for targeted drug delivery, Acta Pharmaceutica Sinica B, 6 (2016) 106-113.
[19] K.M.R. Srivalli, B. Mishra, Drug nanocrystals: A way toward scale-up, Saudi Pharmaceutical Journal, 24 (2016) 386-404.
[20] F. Alexis, E. Pridgen, L.K. Molnar, O.C. Farokhzad, Factors affecting the clearance and

biodistribution of polymeric nanoparticles, Molecular pharmaceutics, 5 (2008) 505-515.
[21] M.A. Dobrovolskaia, P. Aggarwal, J.B. Hall, S.E. McNeil, Preclinical studies to understand nanoparticle interaction with the immune system and its potential effects on nanoparticle biodistribution, Molecular pharmaceutics, 5 (2008) 487-495.
[22] X. Huang, L. Li, T. Liu, N. Hao, H. Liu, D. Chen, F. Tang, The shape effect of mesoporous silica nanoparticles on biodistribution, clearance, and biocompatibility in vivo, ACS nano, 5 (2011) 5390-5399.
[23] R. Karnik, F. Gu, P. Basto, C. Cannizzaro, L. Dean, W. Kyei-Manu, R. Langer, O.C. Farokhzad, Microfluidic platform for controlled synthesis of polymeric nanoparticles, Nano letters, 8 (2008) 2906-2912.
[24] S. Chen, Y.Y.C. Tam, P.J.C. Lin, M.M.H. Sung, Y.K. Tam, P.R. Cullis, Influence of particle size on the in vivo potency of lipid nanoparticle formulations of siRNA, Journal of Controlled Release, 235 (2016) 236-244.
[25] S.G.M. Ong, M. Chitneni, K.S. Lee, L.C. Ming, K.H. Yuen, Evaluation of extrusion technique for nanosizing liposomes, Pharmaceutics, 8 (2016) 36.
[26] D.B. Shelar, S.K. Pawar, P.R. Vavia, Fabrication of isradipine nanosuspension by anti-solvent microprecipitation–high-pressure homogenization method for enhancing dissolution rate and oral bioavailability, Drug delivery and translational research, 3 (2013) 384-391.
[27] Y. Le, H. Ji, J.-F. Chen, Z. Shen, J. Yun, M. Pu, Nanosized bicalutamide and its molecular structure in solvents, International journal of pharmaceutics, 370 (2009) 175-180.
[28] X. Zhang, Q. Xia, N. Gu, Preparation of all-trans retinoic acid nanosuspensions using a modified precipitation method, Drug development and industrial pharmacy, 32 (2006) 857-863.
[29] P.M. Valencia, O.C. Farokhzad, R. Karnik, R. Langer, Microfluidic technologies for accelerating the clinical translation of nanoparticles, Nano-Enabled Medical Applications, (2020) 93-112.
[30] K. Zhai, X. Pei, C. Wang, Y. Deng, Y. Tan, Y. Bai, B. Zhang, K. Xu, P. Wang, Water-in-oil Pickering emulsion polymerization of N-isopropyl acrylamide using starch-based nanoparticles as emulsifier, International Journal of Biological Macromolecules, 131 (2019) 1032-1037.
[31] A. Fabozzi, F. Della Sala, M. di Gennaro, M. Barretta, G. Longobardo, N. Solimando, M. Pagliuca, A. Borzacchiello, Design of functional nanoparticles by microfluidic platforms as advanced drug delivery systems for cancer therapy, Lab on a Chip, (2023).
[32] R.J. Davey, S.L.M. Schroeder, J.H. Ter Horst, Nucleation of organic crystals—a molecular perspective, Angewandte Chemie International Edition, 52 (2013) 2166-2179.
[33] J. Polte, R. Erler, A.F. Thunemann, S. Sokolov, T.T. Ahner, K. Rademann, F. Emmerling, R. Kraehnert, Nucleation and growth of gold nanoparticles studied via in situ small angle X-ray scattering at millisecond time resolution, ACS nano, 4 (2010) 1076-1082.
[34] S. Teychené, B. Biscans, Nucleation kinetics of polymorphs: induction period and interfacial energy measurements, Crystal Growth and Design, 8 (2008) 1133-1139.
[35] N.T.K. Thanh, N. Maclean, S. Mahiddine, Mechanisms of nucleation and growth of nanoparticles in solution, Chemical reviews, 114 (2014) 7610-7630.
[36] H. Yang, M. Svard, J. Zeglinski, Å.C. Rasmuson, Influence of solvent and solid-state structure on nucleation of parabens, Crystal growth & design, 14 (2014) 3890-3902.
[37] D.J. Jin, H.S. Uhm, G. Cho, Influence of the gas-flow Reynolds number on a plasma column in a glass tube, Physics of Plasmas, 20 (2013) 083513.
[38] D. Holzinger, A. Ehresmann, Diffusion enhancement in a laminar flow liquid by near-surface transport of superparamagnetic bead rows, Microfluidics and Nanofluidics, 19 (2015) 395-402.
[39] Y. Shen, S.A. Yuk, S. Kwon, H. Tamam, Y. Yeo, B. Han, A timescale-guided microfluidic synthesis of tannic acid-FeIII network nanocapsules of hydrophobic drugs, Journal of Controlled Release, 357 (2023) 484-497.
[40] K.K.F. Glass, E.K. Longmire, A. Hubel, Optimization of a microfluidic device for diffusion-based extraction of DMSO from a cell suspension, International journal of heat and mass transfer, 51 (2008) 5749-5757.

[41] M. Lu, A. Ozcelik, C.L. Grigsby, Y. Zhao, F. Guo, K.W. Leong, T.J. Huang, Microfluidic hydrodynamic focusing for synthesis of nanomaterials, Nano Today, 11 (2016) 778-792.
[42] D. Holcman, Z. Schuss, Time scale of diffusion in molecular and cellular biology, Journal of Physics A: Mathematical and Theoretical, 47 (2014) 173001.
[43] G.-B. Lee, C.-C. Chang, S.-B. Huang, R.-J. Yang, The hydrodynamic focusing effect inside rectangular microchannels, Journal of Micromechanics and Microengineering, 16 (2006) 1024.
[44] D. Chen, K.T. Love, Y. Chen, A.A. Eltoukhy, C. Kastrup, G. Sahay, A. Jeon, Y. Dong, K.A. Whitehead, D.G. Anderson, Rapid discovery of potent siRNA-containing lipid nanoparticles enabled by controlled microfluidic formulation, Journal of the American Chemical Society, 134 (2012) 6948-6951.
[45] N.M. Belliveau, J. Huft, P.J.C. Lin, S. Chen, A.K.K. Leung, T.J. Leaver, A.W. Wild, J.B. Lee, R.J. Taylor, Y.K. Tam, Microfluidic synthesis of highly potent limit-size lipid nanoparticles for in vivo delivery of siRNA, Molecular Therapy-Nucleic Acids, 1 (2012) e37.
[46] A.D. Stroock, S.K.W. Dertinger, A. Ajdari, I. Mezic, H.A. Stone, G.M. Whitesides, Chaotic mixer for microchannels, Science, 295 (2002) 647-651.
[47] M. Maeki, T. Saito, Y. Sato, T. Yasui, N. Kaji, A. Ishida, H. Tani, Y. Baba, H. Harashima, M. Tokeshi, A strategy for synthesis of lipid nanoparticles using microfluidic devices with a mixer structure, RSC advances, 5 (2015) 46181-46185.
[48] A. Abou-Hassan, O. Sandre, V. Cabuil, Microfluidics in inorganic chemistry, Angewandte Chemie International Edition, 49 (2010) 6268-6286.
[49] S. Thomas, T. Ameel, J. Guilkey, Mixing kinematics of moderate Reynolds number flows in a T-channel, Physics of Fluids, 22 (2010) 013601.
[50] J.A. Kulkarni, Y.Y.C. Tam, S. Chen, Y.K. Tam, J. Zaifman, P.R. Cullis, S. Biswas, Rapid synthesis of lipid nanoparticles containing hydrophobic inorganic nanoparticles, Nanoscale, 9 (2017) 13600-13609.
[51] M.A. Ansari, K.-Y. Kim, K. Anwar, S.M. Kim, Vortex micro T-mixer with non-aligned inputs, Chemical Engineering Journal, 181 (2012) 846-850.
[52] M.A. Ansari, K.-Y. Kim, S.M. Kim, Numerical and experimental study on mixing performances of simple and vortex micro T-mixers, Micromachines, 9 (2018) 204.
[53] Y. Kim, B. Lee Chung, M. Ma, W.J.M. Mulder, Z.A. Fayad, O.C. Farokhzad, R. Langer, Mass production and size control of lipid–polymer hybrid nanoparticles through controlled microvortices, Nano letters, 12 (2012) 3587-3591.
[54] Y. Kim, F. Fay, D.P. Cormode, B.L. Sanchez-Gaytan, J. Tang, E.J. Hennessy, M. Ma, K. Moore, O.C. Farokhzad, E.A. Fisher, Single step reconstitution of multifunctional high-density lipoprotein-derived nanomaterials using microfluidics, ACS nano, 7 (2013) 9975-9983.
[55] M. Rhee, P.M. Valencia, M.I. Rodriguez, R. Langer, O.C. Farokhzad, R. Karnik, Synthesis of size-tunable polymeric nanoparticles enabled by 3D hydrodynamic flow focusing in single-layer microchannels, Advanced Materials, 23 (2011) H79-H83.
[56] X. Luo, P. Su, W. Zhang, C.L. Raston, Microfluidic devices in fabricating nano or micromaterials for biomedical applications, Advanced Materials Technologies, 4 (2019) 1900488.
[57] G. Gkogkos, M.O. Besenhard, L. Storozhuk, N.T.K. Thanh, A. Gavriilidis, Fouling-proof triple stream 3D flow focusing based reactor: Design and demonstration for iron oxide nanoparticle co-precipitation synthesis, Chemical Engineering Science, 251 (2022) 117481.
[58] L. Kong, R. Chen, X. Wang, C.-X. Zhao, Q. Chen, M. Hai, D. Chen, Z. Yang, D.A. Weitz, Controlled co-precipitation of biocompatible colorant-loaded nanoparticles by microfluidics for natural color drinks, Lab on a Chip, 19 (2019) 2089-2095.
[59] R. Othman, G.T. Vladisavljević, H.C.H. Bandulasena, Z.K. Nagy, Production of polymeric nanoparticles by micromixing in a co-flow microfluidic glass capillary device, Chemical Engineering Journal, 280 (2015) 316-329.
[60] J. Wang, W. Chen, J. Sun, C. Liu, Q. Yin, L. Zhang, Y. Xianyu, X. Shi, G. Hu, X. Jiang, A

microfluidic tubing method and its application for controlled synthesis of polymeric nanoparticles, Lab on a Chip, 14 (2014) 1673-1677.
[61] K.-I. Min, H.-J. Lee, D.-P. Kim, Three-dimensional flash flow microreactor for scale-up production of monodisperse PEG–PLGA nanoparticles, Lab on a Chip, 14 (2014) 3987-3992.
[62] D. Desai, Y.A. Guerrero, V. Balachandran, A. Morton, L. Lyon, B. Larkin, D.E. Solomon, Towards a microfluidics platform for the continuous manufacture of organic and inorganic nanoparticles, Nanomedicine: Nanotechnology, Biology and Medicine, 35 (2021) 102402.
[63] D. Prochowicz, A. Kornowicz, J. Lewiński, Interactions of native cyclodextrins with metal ions and inorganic nanoparticles: fertile landscape for chemistry and materials science, Chemical reviews, 117 (2017) 13461-13501.
[64] X. Li, X. Jiang, Microfluidics for producing poly (lactic-co-glycolic acid)-based pharmaceutical nanoparticles, Advanced drug delivery reviews, 128 (2018) 101-114.
[65] H.K. Makadia, S.J. Siegel, Poly lactic-co-glycolic acid (PLGA) as biodegradable controlled drug delivery carrier, Polymers, 3 (2011) 1377-1397.
[66] E. Sah, H. Sah, Recent trends in preparation of poly (lactide-co-glycolide) nanoparticles by mixing polymeric organic solution with antisolvent, Journal of Nanomaterials, 16 (2015) 61-61.
[67] S. Zalba, T.L.M. Ten Hagen, C. Burgui, M.J. Garrido, Stealth nanoparticles in oncology: Facing the PEG dilemma, Journal of Controlled Release, 351 (2022) 22-36.
[68] H.H. Gustafson, D. Holt-Casper, D.W. Grainger, H. Ghandehari, Nanoparticle uptake: the phagocyte problem, Nano today, 10 (2015) 487-510.
[69] N. Kamaly, B. Yameen, J. Wu, O.C. Farokhzad, Degradable controlled-release polymers and polymeric nanoparticles: mechanisms of controlling drug release, Chemical reviews, 116 (2016) 2602-2663.
[70] J. Sun, Y. Xianyu, M. Li, W. Liu, L. Zhang, D. Liu, C. Liu, G. Hu, X. Jiang, A microfluidic origami chip for synthesis of functionalized polymeric nanoparticles, Nanoscale, 5 (2013) 5262-5265.
[71] M.H.M. Leung, A.Q. Shen, Microfluidic assisted nanoprecipitation of PLGA nanoparticles for curcumin delivery to leukemia jurkat cells, Langmuir, 34 (2018) 3961-3970.
[72] S.M. Giannitelli, E. Limiti, P. Mozetic, F. Pinelli, X. Han, F. Abbruzzese, F. Basoli, D. Del Rio, S. Scialla, F. Rossi, Droplet-based microfluidic synthesis of nanogels for controlled drug delivery: tailoring nanomaterial properties via pneumatically actuated flow-focusing junction, Nanoscale, 14 (2022) 11415-11428.
[73] S. Streck, A.J. Clulow, H.M. Nielsen, T. Rades, B.J. Boyd, A. McDowell, The distribution of cell-penetrating peptides on polymeric nanoparticles prepared using microfluidics and elucidated with small angle X-ray scattering, Journal of colloid and interface science, 555 (2019) 438-448.
[74] L. Martín-Banderas, E. Sáez-Fernández, M.Á. Holgado, M.M. Durán-Lobato, J.C. Prados, C. Melguizo, J.L. Arias, Biocompatible gemcitabine-based nanomedicine engineered by Flow Focusing® for efficient antitumor activity, International journal of pharmaceutics, 443 (2013) 103-109.
[75] L. Sercombe, T. Veerati, F. Moheimani, S.Y. Wu, A.K. Sood, S. Hua, Advances and challenges of liposome assisted drug delivery, Frontiers in pharmacology, 6 (2015) 286.
[76] M.J.W. Evers, J.A. Kulkarni, R. van der Meel, P.R. Cullis, P. Vader, R.M. Schiffelers, State-of-the-art design and rapid-mixing production techniques of lipid nanoparticles for nucleic acid delivery, Small Methods, 2 (2018) 1700375.
[77] Y. Sato, Y. Note, M. Maeki, N. Kaji, Y. Baba, M. Tokeshi, H. Harashima, Elucidation of the physicochemical properties and potency of siRNA-loaded small-sized lipid nanoparticles for siRNA delivery, Journal of controlled release, 229 (2016) 48-57.
[78] Y. Zhu, R. Shen, I. Vuong, R.A. Reynolds, M.J. Shears, Z.-C. Yao, Y. Hu, W.J. Cho, J. Kong, S.K. Reddy, Multi-step screening of DNA/lipid nanoparticles and co-delivery with siRNA to enhance and prolong gene expression, Nature communications, 13 (2022) 4282.

[79] R.L. Ball, K.A. Hajj, J. Vizelman, P. Bajaj, K.A. Whitehead, Lipid Nanoparticle Formulations for Enhanced Co-delivery of siRNA and mRNA, Nano Letters, 18 (2018) 3814-3822.
[80] P.M. Valencia, P.A. Basto, L. Zhang, M. Rhee, R. Langer, O.C. Farokhzad, R. Karnik, Single-step assembly of homogenous lipid− polymeric and lipid− quantum dot nanoparticles enabled by microfluidic rapid mixing, ACS nano, 4 (2010) 1671-1679.
[81] D. Xia, Y. He, Q. Li, C. Hu, W. Huang, Y. Zhang, F. Wan, C. Wang, Y. Gan, Transport mechanism of lipid covered saquinavir pure drug nanoparticles in intestinal epithelium, Journal of Controlled Release, 269 (2018) 159-170.
[82] Y. Wu, B. Yu, A. Jackson, W. Zha, L.J. Lee, B.E. Wyslouzil, Coaxial electrohydrodynamic spraying: a novel one-step technique to prepare oligodeoxynucleotide encapsulated lipoplex nanoparticles, Molecular pharmaceutics, 6 (2009) 1371-1379.
[83] J. Sun, L. Zhang, J. Wang, Q. Feng, D. Liu, Q. Yin, D. Xu, Y. Wei, B. Ding, X. Shi, Tunable rigidity of (polymeric core)-(lipid shell) nanoparticles for regulated cellular uptake, Advanced materials (deerfield beach, fla.), 27 (2014) 1402-1407.
[84] S. Veeranarayanan, T. Maekawa, External stimulus responsive inorganic nanomaterials for cancer theranostics, Advanced Drug Delivery Reviews, 138 (2019) 18-40.
[85] A.C. Anselmo, S. Mitragotri, A review of clinical translation of inorganic nanoparticles, The AAPS journal, 17 (2015) 1041-1054.
[86] N. Hao, Y. Nie, J.X.J. Zhang, Microfluidic synthesis of functional inorganic micro-/nanoparticles and applications in biomedical engineering, International Materials Reviews, 63 (2018) 461-487.
[87] J. Shen, M. Shafiq, M. Ma, H. Chen, Synthesis and surface engineering of inorganic nanomaterials based on microfluidic technology, Nanomaterials, 10 (2020) 1177.
[88] A. Meola, J. Rao, N. Chaudhary, M. Sharma, S.D. Chang, Gold nanoparticles for brain tumor imaging: A systematic review, Frontiers in neurology, 9 (2018) 328.
[89] H.B. Ruttala, T. Ramasamy, B.K. Poudel, R.R.T. Ruttala, S.G. Jin, H.-G. Choi, S.-K. Ku, C.S. Yong, J.O. Kim, Multi-responsive albumin-lonidamine conjugated hybridized gold nanoparticle as a combined photothermal-chemotherapy for synergistic tumor ablation, Acta Biomaterialia, 101 (2020) 531-543.
[90] M. Malki, A. Shapira, T. Dvir, Chondroitin sulfate-AuNRs electroactive scaffolds for on-demand release of biofactors, Journal of Nanobiotechnology, 20 (2022) 1-9.
[91] I. Ternad, S. Penninckx, V. Lecomte, T. Vangijzegem, L. Conrard, S. Lucas, A.-C. Heuskin, C. Michiels, R.N. Muller, D. Stanicki, Advances in the Mechanistic Understanding of Iron Oxide Nanoparticles' Radiosensitizing Properties, Nanomaterials, 13 (2023) 201.
[92] A. Setia, A.K. Mehata, A.K. Malik, M.K. Viswanadh, M.S. Muthu, Theranostic magnetic nanoparticles: Synthesis, properties, toxicity, and emerging trends for biomedical applications, Journal of Drug Delivery Science and Technology, (2023) 104295.
[93] A. Włodarczyk, S. Gorgoń, A. Radoń, K. Bajdak-Rusinek, Magnetite Nanoparticles in Magnetic Hyperthermia and Cancer Therapies: Challenges and Perspectives, Nanomaterials, 12 (2022) 1807.
[94] A.A. Demessie, Y. Park, P. Singh, A.S. Moses, T. Korzun, F.Y. Sabei, H.A. Albarqi, L. Campos, C.R. Wyatt, K. Farsad, An Advanced Thermal Decomposition Method to Produce Magnetic Nanoparticles with Ultrahigh Heating Efficiency for Systemic Magnetic Hyperthermia, Small Methods, 6 (2022) 2200916.
[95] Y. Chen, H. Chen, M. Ma, F. Chen, L. Guo, L. Zhang, J. Shi, Double mesoporous silica shelled spherical/ellipsoidal nanostructures: synthesis and hydrophilic/hydrophobic anticancer drug delivery, Journal of Materials Chemistry, 21 (2011) 5290-5298.
[96] A.A. Alhowyan, M.A. Kalam, M. Iqbal, M. Raish, A.M. El-Toni, M. Alkholief, A.A. Almomen, A. Alshamsan, Mesoporous silica nanoparticles coated with carboxymethyl chitosan for 5-fluorouracil ocular delivery: characterization, in vitro and in vivo studies, Molecules, 28 (2023) 1260.
[97] J. Yan, X. Xu, J. Zhou, C. Liu, L. Zhang, D. Wang, F. Yang, H. Zhang, Fabrication of a pH/redox-triggered mesoporous silica-based nanoparticle with microfluidics for anticancer drugs doxorubicin and paclitaxel codelivery, ACS Applied Bio Materials, 3 (2020) 1216-

1225.
[98] O. Kašpar, A.H. Koyuncu, A. Pittermannová, P. Ulbrich, V. Tokárová, Governing factors for preparation of silver nanoparticles using droplet-based microfluidic device, Biomedical Microdevices, 21 (2019) 1-14.
[99] L.L. Lazarus, C.T. Riche, B.C. Marin, M. Gupta, N. Malmstadt, R.L. Brutchey, Two-phase microfluidic droplet flows of ionic liquids for the synthesis of gold and silver nanoparticles, ACS applied materials & interfaces, 4 (2012) 3077-3083.
[100] S.J. Shepherd, D. Issadore, M.J. Mitchell, Microfluidic formulation of nanoparticles for biomedical applications, Biomaterials, (2021) 120826.
[101] Z. Liu, Y. Li, W. Li, C. Xiao, D. Liu, C. Dong, M. Zhang, E. Mäkilä, M. Kemell, J. Salonen, Multifunctional nanohybrid based on porous silicon nanoparticles, gold nanoparticles, and acetalated dextran for liver regeneration and acute liver failure theranostics, Advanced Materials, 30 (2018) 1703393.
[102] L. Rao, B. Cai, L.-L. Bu, Q.-Q. Liao, S.-S. Guo, X.-Z. Zhao, W.-F. Dong, W. Liu, Microfluidic electroporation-facilitated synthesis of erythrocyte membrane-coated magnetic nanoparticles for enhanced imaging-guided cancer therapy, Acs Nano, 11 (2017) 3496-3505.
[103] S. Kalepu, V. Nekkanti, Insoluble drug delivery strategies: review of recent advances and business prospects, Acta Pharmaceutica Sinica B, 5 (2015) 442-453.
[104] B. Sinha, R.H. Müller, J.P. Möschwitzer, Bottom-up approaches for preparing drug nanocrystals: formulations and factors affecting particle size, International journal of pharmaceutics, 453 (2013) 126-141.
[105] J. Tao, S.F. Chow, Y. Zheng, Application of flash nanoprecipitation to fabricate poorly water-soluble drug nanoparticles, Acta pharmaceutica sinica B, 9 (2019) 4-18.
[106] A. Tuomela, J. Hirvonen, L. Peltonen, Stabilizing agents for drug nanocrystals: effect on bioavailability, Pharmaceutics, 8 (2016) 16.
[107] J. Xie, Y. Luo, Y. Liu, Y. Ma, P. Yue, M. Yang, Novel redispersible nanosuspensions stabilized by co-processed nanocrystalline cellulose–sodium carboxymethyl starch for enhancing dissolution and oral bioavailability of baicalin, International journal of nanomedicine, 14 (2019) 353.
[108] Y. Aidana, Y. Wang, J. Li, S. Chang, K. Wang, D.-G. Yu, Fast dissolution electrospun medicated nanofibers for effective delivery of poorly water-soluble drug, Current drug delivery, 19 (2022) 422-435.
[109] C.P. Feliciano, K. Tsuboi, K. Suzuki, H. Kimura, Y. Nagasaki, Long-term bioavailability of redox nanoparticles effectively reduces organ dysfunctions and death in whole-body irradiated mice, Biomaterials, 129 (2017) 68-82.
[110] B.-Q. Chen, Y. Zhao, Y. Zhang, Y.-J. Pan, H.-Y. Xia, R.K. Kankala, S.-B. Wang, G. Liu, A.-Z. Chen, Immune-regulating camouflaged nanoplatforms: A promising strategy to improve cancer nano-immunotherapy, Bioactive Materials, 21 (2023) 1-19.
[111] J.H. Lee, Y. Yeo, Controlled drug release from pharmaceutical nanocarriers, Chemical engineering science, 125 (2015) 75-84.
[112] W. Zuo, D. Chen, Z. Fan, L. Chen, Z. Zhu, Q. Zhu, X. Zhu, Design of light/ROS cascade-responsive tumor-recognizing nanotheranostics for spatiotemporally controlled drug release in locoregional photo-chemotherapy, Acta Biomaterialia, 111 (2020) 327-340.
[113] H. Guo, J. Huang, Y. Tan, W. Wu, T. Huang, N. Zhang, S. Chen, C. Zhang, X. Xie, X. Shuai, Nanodrug shows spatiotemporally controlled release of anti-PD-L1 antibody and STING agonist to effectively inhibit tumor progression after radiofrequency ablation, Nano Today, 43 (2022) 101425.
[114] C.J. Gil, L. Li, B. Hwang, M. Cadena, A.S. Theus, T.A. Finamore, H. Bauser-Heaton, M. Mahmoudi, R.K. Roeder, V. Serpooshan, Tissue engineered drug delivery vehicles: Methods to monitor and regulate the release behavior, Journal of Controlled Release, 349 (2022) 143-155.
[115] S. Sharma, A. Verma, G. Pandey, N. Mittapelly, P.R. Mishra, Investigating the role of Pluronic-g-Cationic polyelectrolyte as functional stabilizer for nanocrystals: Impact on

Paclitaxel oral bioavailability and tumor growth, Acta Biomaterialia, 26 (2015) 169-183.
[116] L. Gao, G. Liu, J. Ma, X. Wang, L. Zhou, X. Li, Drug nanocrystals: in vivo performances, Journal of controlled release, 160 (2012) 418-430.
[117] M.L. Branham, T. Moyo, T. Govender, Preparation and solid-state characterization of ball milled saquinavir mesylate for solubility enhancement, European journal of pharmaceutics and biopharmaceutics, 80 (2012) 194-202.
[118] S. Sultana, S. Talegaonkar, R. Ali, G. Mittal, F.J. Ahmad, A. Bhatnagar, Inhalation of alendronate nanoparticles as dry powder inhaler for the treatment of osteoporosis, Journal of microencapsulation, 29 (2012) 445-454.
[119] Y. Lv, W. Wu, C.D. Corpstein, T. Li, Y. Lu, Biological and intracellular fates of drug nanocrystals through different delivery routes: Recent development enabled by bioimaging and PK modeling, Advanced Drug Delivery Reviews, (2022) 114466.
[120] X. Miao, W. Yang, T. Feng, J. Lin, P. Huang, Drug nanocrystals for cancer therapy, Wiley Interdisciplinary Reviews: Nanomedicine and Nanobiotechnology, 10 (2018) e1499.
[121] H. Yang, F. Teng, P. Wang, B. Tian, X. Lin, X. Hu, L. Zhang, K. Zhang, Y. Zhang, X. Tang, Investigation of a nanosuspension stabilized by Soluplus® to improve bioavailability, International journal of pharmaceutics, 477 (2014) 88-95.
[122] H. Zhao, J.-X. Wang, Q.-A. Wang, J.-F. Chen, J. Yun, Controlled liquid antisolvent precipitation of hydrophobic pharmaceutical nanoparticles in a microchannel reactor, Industrial & Engineering Chemistry Research, 46 (2007) 8229-8235.
[123] J.-X. Wang, Q.-X. Zhang, Y. Zhou, L. Shao, J.-F. Chen, Microfluidic synthesis of amorphous cefuroxime axetil nanoparticles with size-dependent and enhanced dissolution rate, Chemical Engineering Journal, 162 (2010) 844-851.
[124] H.-X. Zhang, J.-X. Wang, L. Shao, J.-F. Chen, Microfluidic fabrication of monodispersed pharmaceutical colloidal spheres of atorvastatin calcium with tunable sizes, Industrial & engineering chemistry research, 49 (2010) 4156-4161.
[125] V. Génot, S. Desportes, C. Croushore, J.-P. Lefèvre, R.B. Pansu, J.A. Delaire, P.R. von Rohr, Synthesis of organic nanoparticles in a 3D flow focusing microreactor, Chemical Engineering Journal, 161 (2010) 234-239.
[126] D. Liu, H. Zhang, S. Cito, J. Fan, E. Mäkilä, J. Salonen, J. Hirvonen, T.M. Sikanen, D.A. Weitz, H.I.A. Santos, Core/shell nanocomposites produced by superfast sequential microfluidic nanoprecipitation, Nano letters, 17 (2017) 606-614.
[127] Z. Liu, Y. Huang, Y. Jin, Y. Cheng, Mixing intensification by chaotic advection inside droplets for controlled nanoparticle preparation, Microfluidics and nanofluidics, 9 (2010) 773-786.
[128] G. Shen, R. Xing, N. Zhang, C. Chen, G. Ma, X. Yan, Interfacial cohesion and assembly of bioadhesive molecules for design of long-term stable hydrophobic nanodrugs toward effective anticancer therapy, ACS nano, 10 (2016) 5720-5729.
[129] J. Li, Y. Zhou, J. Liu, X. Yang, K. Zhang, L. Lei, H. Hu, H. Zhang, L. Ouyang, H. Gao, Metal-phenolic networks with ferroptosis to deliver NIR-responsive CO for synergistic therapy, Journal of Controlled Release, 352 (2022) 313-327.
[130] Y. Chen, W. Xu, M. Shafiq, D. Song, T. Wang, Z. Yuan, X. Xie, X. Yu, Y. Shen, B. Sun, Injectable nanofiber microspheres modified with metal phenolic networks for effective osteoarthritis treatment, Acta Biomaterialia, 157 (2023) 593-608.
[131] H. Ejima, J.J. Richardson, K. Liang, J.P. Best, M.P. van Koeverden, G.K. Such, J. Cui, F. Caruso, One-step assembly of coordination complexes for versatile film and particle engineering, Science, 341 (2013) 154-157.
[132] C. Gao, Y. Wang, Z. Ye, Z. Lin, X. Ma, Q. He, Biomedical Micro-/Nanomotors: From Overcoming Biological Barriers to In Vivo Imaging, Advanced Materials, 33 (2021) 2000512.
[133] Y. Ping, J. Guo, H. Ejima, X. Chen, J.J. Richardson, H. Sun, F. Caruso, pH-responsive capsules engineered from metal-phenolic networks for anticancer drug delivery, Small, 11 (2015) 2032-2036.
[134] S.A. Abouelmagd, N.H. Abd Ellah, O. Amen, A. Abdelmoez, N.G. Mohamed, Self-assembled

tannic acid complexes for pH-responsive delivery of antibiotics: role of drug-carrier interactions, International journal of pharmaceutics, 562 (2019) 76-85.
[135] Z. He, Y. Hu, Z. Gui, Y. Zhou, T. Nie, J. Zhu, Z. Liu, K. Chen, L. Liu, K.W. Leong, Sustained release of exendin-4 from tannic acid/Fe (III) nanoparticles prolongs blood glycemic control in a mouse model of type II diabetes, Journal of Controlled Release, 301 (2019) 119-128.
[136] W. Li, W. Bing, S. Huang, J. Ren, X. Qu, Mussel Byssus-Like Reversible Metal-Chelated Supramolecular Complex Used for Dynamic Cellular Surface Engineering and Imaging, Advanced Functional Materials, 25 (2015) 3775-3784.
[137] D. Su, X. Liu, L. Wang, C. Ma, H. Xie, H. Zhang, X. Meng, Y. Huang, X. Huang, Bio-inspired engineering proteinosomes with a cell-wall-like protective shell by self-assembly of a metal-chelated complex, Chemical Communications, 52 (2016) 13803-13806.
[138] J. Lee, H. Cho, J. Choi, D. Kim, D. Hong, J.H. Park, S.H. Yang, I.S. Choi, Chemical sporulation and germination: cytoprotective nanocoating of individual mammalian cells with a degradable tannic acid–Fe III complex, Nanoscale, 7 (2015) 18918-18922.
[139] M.S. Taha, G.M. Cresswell, J. Park, W. Lee, T.L. Ratliff, Y. Yeo, Sustained delivery of carfilzomib by tannic acid-based nanocapsules helps develop antitumor immunity, Nano letters, 19 (2019) 8333-8341.
[140] S.A. Yuk, H. Kim, N.S. Abutaleb, A.M. Dieterly, M.S. Taha, M.D. Tsifansky, L.T. Lyle, M.N. Seleem, Y. Yeo, Nanocapsules modify membrane interaction of polymyxin B to enable safe systemic therapy of Gram-negative sepsis, Science Advances, 7 (2021) eabj1577.
[141] Y. Chen, D. Jia, Q. Wang, Y. Sun, Z. Rao, X. Lei, J. Zhao, K. Zeng, Z. Xu, J. Ming, Promotion of the anticancer activity of curcumin based on a metal–polyphenol networks delivery system, International Journal of Pharmaceutics, 602 (2021) 120650.
[142] P. Liu, X. Liu, Y. Cheng, S. Zhong, X. Shi, S. Wang, M. Liu, J. Ding, W. Zhou, Core–Shell Nanosystems for Self-Activated Drug–Gene Combinations against Triple-Negative Breast Cancer, ACS Applied Materials & Interfaces, 12 (2020) 53654-53664.
[143] Y. Liu, K. Ma, T. Jiao, R. Xing, G. Shen, X. Yan, Water-insoluble photosensitizer nanocolloids stabilized by supramolecular interfacial assembly towards photodynamic therapy, Scientific reports, 7 (2017) 1-8.
[144] F. Taemaitree, Y. Koseki, N. Saito, R. Suzuki, A.T.N. Dao, H. Kasai, Self-assemble tannic acid and iron complexes on pure nanodrugs surface prevents aggregation and enhances anticancer drug delivery efficiency, Molecular Crystals and Liquid Crystals, 706 (2020) 116-121.
[145] F. Huang, X. Jiang, M.A. Sallam, X. Zhang, W. He, A Nanocrystal Platform Based on Metal-Phenolic Network Wrapping for Drug Solubilization, AAPS PharmSciTech, 23 (2022) 1-11.
[146] M. Mu, X. Liang, D. Chuan, S. Zhao, W. Yu, R. Fan, A. Tong, N. Zhao, B. Han, G. Guo, Chitosan coated pH-responsive metal-polyphenol delivery platform for melanoma chemotherapy, Carbohydrate Polymers, 264 (2021) 118000.
[147] H.S.M. Ali, P. York, A.M.A. Ali, N. Blagden, Hydrocortisone nanosuspensions for ophthalmic delivery: a comparative study between microfluidic nanoprecipitation and wet milling, Journal of controlled release, 149 (2011) 175-181.
[148] S.D. Ibsen, J. Wright, J.M. Lewis, S. Kim, S.Y. Ko, J. Ong, S. Manouchehri, A. Vyas, J. Akers, C.C. Chen, B.S. Carter, S.C. Esener, M.J. Heller, Rapid Isolation and Detection of Exosomes and Associated Biomarkers from Plasma, Acs Nano, 11 (2017) 6641-6651.
[149] V. Chaurey, A. Rohani, Y.H. Su, K.T. Liao, C.F. Chou, N.S. Swami, Scaling down constriction-based (electrodeless) dielectrophoresis devices for trapping nanoscale bioparticles in physiological media of high-conductivity, Electrophoresis, 34 (2013) 1097-1104.
[150] M. Dimaki, M.H. Olsen, N. Rozlosnik, W.E. Svendsen, Sub-100 nm Nanoparticle Upconcentration in Flow by Dielectrophoretic Forces, Micromachines, 13 (2022).
[151] C. Liu, J.Y. Guo, F. Tian, N. Yang, F.S. Yan, Y.P. Ding, J.Y. Wei, G.Q. Hu, G.J. Nie, J.S. Sun, Field-Free Isolation of Exosomes from Extracellular Vesicles by Microfluidic Viscoelastic Flows, Acs Nano, 11 (2017) 6968-6976.
[152] B.H. Wunsch, J.T. Smith, S.M. Gifford, C. Wang, M. Brink, R.L. Bruce, R.H. Austin, G.

Stolovitzky, Y. Astier, Nanoscale lateral displacement arrays for the separation of exosomes and colloids down to 20 nm, Nature nanotechnology, 11 (2016) 936-940.
[153] H. Bruus, Acoustofluidics 7: The acoustic radiation force on small particles, Lab on a Chip, 12 (2012) 1014-1021.
[154] A.N. Morozov, W. van Saarloos, An introductory essay on subcritical instabilities and the transition to turbulence in visco-elastic parallel shear flows, Physics Reports-Review Section of Physics Letters, 447 (2007) 112-143.
[155] D.Y. Li, W.C. Yu, T. Zhou, M.Q. Li, Y.X. Song, D.Q. Li, Conductivity-difference-enhanced DC dielectrophoretic particle separation in a microfluidic chip, Analyst, 147 (2022) 1106-1116.
[156] W.J. Zhao, L.Q. Zhang, Y.F. Ye, Y.A. Li, X.F. Luan, J.L. Liu, J. Cheng, Y. Zhao, M.X. Li, C.J. Huang, Microsphere mediated exosome isolation and ultra-sensitive detection on a dielectrophoresis integrated microfluidic device, Analyst, 146 (2021) 5962-5972.
[157] S. Ayala-Mar, V.H. Perez-Gonzalez, M.A. Mata-Gomez, R.C. Gallo-Villanueva, J. Gonzalez-Valdez, Electrokinetically Driven Exosome Separation and Concentration Using Dielectrophoretic-Enhanced PDMS-Based Microfluidics, Analytical Chemistry, 91 (2019) 14975-14982.
[158] T.M. Squires, S.R. Quake, Microfluidics: Fluid physics at the nanoliter scale, Reviews of Modern Physics, 77 (2005) 977-1026.
[159] D. Di Carlo, Inertial microfluidics, Lab on a Chip, 9 (2009) 3038-3046.
[160] H. Amini, W. Lee, D. Di Carlo, Inertial microfluidic physics, Lab on a Chip, 14 (2014) 2739-2761.
[161] S.W. Choe, B. Kim, M. Kim, Progress of Microfluidic Continuous Separation Techniques for Micro-/Nanoscale Bioparticles, Biosensors (Basel), 11 (2021).
[162] P. Su, C.H. Ren, Y.S. Fu, J.H. Guo, J.C. Guo, Q. Yuan, Magnetophoresis in microfluidic lab: Recent advance, Sensors and Actuators a-Physical, 332 (2021).
[163] C. Zhang, K. Khoshmanesh, A. Mitchell, K. Kalantar-zadeh, Dielectrophoresis for manipulation of micro/nano particles in microfluidic systems, Analytical and Bioanalytical Chemistry, 396 (2010) 401-420.
[164] Y. Gao, M.R. Wu, Y. Lin, J. Xu, Acoustic Microfluidic Separation Techniques and Bioapplications: A Review, Micromachines, 11 (2020).
[165] Y. Yang, L. Zhang, K. Jin, M. He, W. Wei, X. Chen, Q. Yang, Y. Wang, W. Pang, X. Ren, Self-adaptive virtual microchannel for continuous enrichment and separation of nanoparticles, Science Advances, 8 (2022) eabn8440.
[166] S. Hettiarachchi, H. Cha, L. Ouyang, A. Mudugamuwa, H. An, G. Kijanka, N. Kashaninejad, N.-T. Nguyen, J. Zhang, Recent microfluidic advances in submicron to nanoparticle manipulation and separation, Lab on a Chip, (2023).
[167] H. Hu, G. Cai, Z. Gao, C. Liang, F. Yang, X. Dou, C. Jia, J. Zhao, S. Feng, B. Li, A microfluidic immunosensor for automatic detection of carcinoembryonic antigen based on immunomagnetic separation and droplet arrays, Analyst, 148 (2023) 1939-1947.
[168] C.A. Hermann, M. Mayer, C. Griesche, F. Beck, A.J. Baeumner, Microfluidic-enabled magnetic labelling of nanovesicles for bioanalytical applications, Analyst, 146 (2021) 997-1003.
[169] Y. Gu, C. Chen, Z. Mao, H. Bachman, R. Becker, J. Rufo, Z. Wang, P. Zhang, J. Mai, S. Yang, Acoustofluidic centrifuge for nanoparticle enrichment and separation, Science advances, 7 (2021) eabc0467.
[170] J. Rufo, F. Cai, J. Friend, M. Wiklund, T.J. Huang, Acoustofluidics for biomedical applications, Nature Reviews Methods Primers, 2 (2022) 30.
[171] S. Zhao, M. Wu, S. Yang, Y. Wu, Y. Gu, C. Chen, J. Ye, Z. Xie, Z. Tian, H. Bachman, A disposable acoustofluidic chip for nano/microparticle separation using unidirectional acoustic transducers, Lab on a Chip, 20 (2020) 1298-1308.
[172] C. Liu, J. Guo, F. Tian, N. Yang, F. Yan, Y. Ding, J. Wei, G. Hu, G. Nie, J. Sun, Field-free isolation of exosomes from extracellular vesicles by microfluidic viscoelastic flows, ACS nano, 11 (2017) 6968-6976.
[173] C. Liu, J. Zhao, F. Tian, J. Chang, W. Zhang, J. Sun, λ-DNA-and aptamer-mediated sorting

and analysis of extracellular vesicles, Journal of the American Chemical Society, 141 (2019) 3817-3821.
[174] M. Asghari, X. Cao, B. Mateescu, D. Van Leeuwen, M.K. Aslan, S. Stavrakis, A.J. deMello, Oscillatory viscoelastic microfluidics for efficient focusing and separation of nanoscale species, ACS nano, 14 (2019) 422-433.
[175] S. Ayala-Mar, V.H. Perez-Gonzalez, M.A. Mata-Gómez, R.C. Gallo-Villanueva, J. González-Valdez, Electrokinetically driven exosome separation and concentration using dielectrophoretic-enhanced PDMS-based microfluidics, Analytical chemistry, 91 (2019) 14975-14982.
[176] M. Dimaki, M.H. Olsen, N. Rozlosnik, W.E. Svendsen, Sub–100 nm Nanoparticle Upconcentration in Flow by Dielectrophoretic Forces, Micromachines, 13 (2022) 866.
[177] K.T. Gustafson, K.T. Huynh, D. Heineck, J. Bueno, A. Modestino, S. Kim, A. Gower, R. Armstrong, C.E. Schutt, S.D. Ibsen, Automated fluorescence quantification of extracellular vesicles collected from blood plasma using dielectrophoresis, Lab on a Chip, 21 (2021) 1318-1332.
[178] J.H. Moore, W.B. Varhue, Y.-H. Su, S.S. Linton, V. Farmehini, T.E. Fox, G.L. Matters, M. Kester, N.S. Swami, Conductance-based biophysical distinction and microfluidic enrichment of nanovesicles derived from pancreatic tumor cells of varying invasiveness, Analytical chemistry, 91 (2019) 10424-10431.
[179] R. Salemmilani, M. Moskovits, C.D. Meinhart, Microfluidic analysis of fentanyl-laced heroin samples by surface-enhanced Raman spectroscopy in a hydrophobic medium, Analyst, 144 (2019) 3080-3087.
[180] T. Salafi, Y. Zhang, Y. Zhang, A review on deterministic lateral displacement for particle separation and detection, Nano-Micro Letters, 11 (2019) 1-33.
[181] D. Li, W. Yu, T. Zhou, M. Li, Y. Song, D. Li, Conductivity-difference-enhanced DC dielectrophoretic particle separation in a microfluidic chip, Analyst, 147 (2022) 1106-1116.
[182] W. Zhao, L. Zhang, Y. Ye, Y. Li, X. Luan, J. Liu, J. Cheng, Y. Zhao, M. Li, C. Huang, Microsphere mediated exosome isolation and ultra-sensitive detection on a dielectrophoresis integrated microfluidic device, Analyst, 146 (2021) 5962-5972.
[183] A. Shakeri, S. Khan, T.F. Didar, Conventional and emerging strategies for the fabrication and functionalization of PDMS-based microfluidic devices, Lab on a Chip, 21 (2021) 3053-3075.
[184] J. Zhou, A.V. Ellis, N.H. Voelcker, Recent developments in PDMS surface modification for microfluidic devices, Electrophoresis, 31 (2010) 2-16.
[185] K.J. Regehr, M. Domenech, J.T. Koepsel, K.C. Carver, S.J. Ellison-Zelski, W.L. Murphy, L.A. Schuler, E.T. Alarid, D.J. Beebe, Biological implications of polydimethylsiloxane-based microfluidic cell culture, Lab on a Chip, 9 (2009) 2132-2139.
[186] M. Radisic, P. Loskill, Beyond PDMS and membranes: new materials for organ-on-a-chip devices, in, ACS Publications, 2021, pp. 2861-2863.
[187] S.B. Campbell, Q. Wu, J. Yazbeck, C. Liu, S. Okhovatian, M. Radisic, Beyond polydimethylsiloxane: alternative materials for fabrication of organ-on-a-chip devices and microphysiological systems, ACS biomaterials science & engineering, 7 (2020) 2880-2899.
[188] J. Nie, J. Fu, Y. He, Hydrogels: the next generation body materials for microfluidic chips?, Small, 16 (2020) 2003797.
[189] Q. Zhao, H. Cui, Y. Wang, X. Du, Microfluidic platforms toward rational material fabrication for biomedical applications, Small, 16 (2020) 1903798.
[190] S. Brittman, S.Z. Oener, K. Guo, H. Āboliņš, A.F. Koenderink, E.C. Garnett, Controlling crystallization to imprint nanophotonic structures into halide perovskites using soft lithography, Journal of Materials Chemistry C, 5 (2017) 8301-8307.
[191] W. Wang, Y.Q. Liu, Y. Liu, B. Han, H. Wang, D.D. Han, J.N. Wang, Y.L. Zhang, H.B. Sun, Direct laser writing of superhydrophobic PDMS elastomers for controllable manipulation via Marangoni effect, Advanced Functional Materials, 27 (2017) 1702946.
[192] W. Li, D. Kitagawa, S. Kobatake, E. Bekyarova, C.J. Bardeen, Patterning submicron photomechanical features into single diarylethene crystals using electron beam lithography, Nanoscale Horizons, 7 (2022) 1065-1072.

[193] D. Ebert, B. Bhushan, Transparent, superhydrophobic, and wear-resistant surfaces using deep reactive ion etching on PDMS substrates, Journal of colloid and interface science, 481 (2016) 82-90.
[194] G. Gonzalez, A. Chiappone, K. Dietliker, C.F. Pirri, I. Roppolo, Fabrication and Functionalization of 3D Printed Polydimethylsiloxane-Based Microfluidic Devices Obtained through Digital Light Processing, Advanced Materials Technologies, 5 (2020) 2000374.
[195] M. Li, S. Li, J. Wu, W. Wen, W. Li, G. Alici, A simple and cost-effective method for fabrication of integrated electronic-microfluidic devices using a laser-patterned PDMS layer, Microfluidics and nanofluidics, 12 (2012) 751-760.
[196] S.J. Shepherd, C.C. Warzecha, S. Yadavali, R. El-Mayta, M.-G. Alameh, L. Wang, D. Weissman, J.M. Wilson, D. Issadore, M.J. Mitchell, Scalable mRNA and siRNA lipid nanoparticle production using a parallelized microfluidic device, Nano Letters, 21 (2021) 5671-5680.
[197] A. Giorello, A. Nicastro, C.L.A. Berli, Microfluidic Platforms for the Production of Nanoparticles at Flow Rates Larger Than One Liter Per Hour, Advanced Materials Technologies, 7 (2022) 2101588.
[198] M. Sheybanifard, L.P.B. Guerzoni, A. Omidinia-Anarkoli, L. De Laporte, J. Buyel, R. Besseling, M. Damen, A. Gerich, T. Lammers, J.M. Metselaar, Liposome manufacturing under continuous flow conditions: towards a fully integrated set-up with in-line control of critical quality attributes, Lab on a Chip, 23 (2023) 182-194.
[199] C. Webb, S. Ip, N.V. Bathula, P. Popova, S.K.V. Soriano, H.H. Ly, B. Eryilmaz, V.A. Nguyen Huu, R. Broadhead, M. Rabel, Current status and future perspectives on MRNA drug manufacturing, Molecular Pharmaceutics, 19 (2022) 1047-1058.
[200] J.W. Shreffler, J.E. Pullan, K.M. Dailey, S. Mallik, A.E. Brooks, Overcoming hurdles in nanoparticle clinical translation: The influence of experimental design and surface modification, International Journal of Molecular Sciences, 20 (2019) 6056.
[201] F. Benfenati, G. Lanzani, Clinical translation of nanoparticles for neural stimulation, Nature Reviews Materials, 6 (2021) 1-4.
[202] N. Kamaly, Z. Xiao, P.M. Valencia, A.F. Radovic-Moreno, O.C. Farokhzad, Targeted polymeric therapeutic nanoparticles: design, development and clinical translation, Chemical Society Reviews, 41 (2012) 2971-3010.
[203] S. Damiati, U.B. Kompella, S.A. Damiati, R. Kodzius, Microfluidic devices for drug delivery systems and drug screening, Genes, 9 (2018) 103.
[204] K. Duval, H. Grover, L.-H. Han, Y. Mou, A.F. Pegoraro, J. Fredberg, Z. Chen, Modeling physiological events in 2D vs. 3D cell culture, Physiology, 32 (2017) 266-277.
[205] M. Ravi, V. Paramesh, S.R. Kaviya, E. Anuradha, F.D.P. Solomon, 3D cell culture systems: advantages and applications, Journal of cellular physiology, 230 (2015) 16-26.
[206] A. Ozcelikkale, H.r. Moon, M. Linnes, B. Han, In vitro microfluidic models of tumor microenvironment to screen transport of drugs and nanoparticles, Wiley Interdisciplinary Reviews: Nanomedicine and Nanobiotechnology, 9 (2017) e1460.
[207] A. Ozcelikkale, K. Shin, V. Noe-Kim, B.D. Elzey, Z. Dong, J.-T. Zhang, K. Kim, I.C. Kwon, K. Park, B. Han, Differential response to doxorubicin in breast cancer subtypes simulated by a microfluidic tumor model, Journal of Controlled Release, 266 (2017) 129-139.
[208] H.-r. Moon, A. Ozcelikkale, Y. Yang, B.D. Elzey, S.F. Konieczny, B. Han, An engineered pancreatic cancer model with intra-tumoral heterogeneity of driver mutations, Lab on a Chip, 20 (2020) 3720-3732.
[209] B. Kwak, A. Ozcelikkale, C.S. Shin, K. Park, B. Han, Simulation of complex transport of nanoparticles around a tumor using tumor-microenvironment-on-chip, Journal of Controlled Release, 194 (2014) 157-167.